Evaluation of Northern Hemisphere blocking climatology in the Global Environment Multiscale (GEM) model and in the present and future climate as simulated by the CMIP5 models

Etienne Dunn-Sigouin

Master of Science

Department of Atmospheric and Oceanic Sciences

McGill University
Montreal, Canada

July 27, 2012

A thesis submitted to the Faculty of Graduate Studies and Research in partial fulfillment of the requirements for the degree of Master of Science

Acknowledgements

First I would like to thank my advisor Professor Seok-Woo Son whose guidance and support made the completion of this work possible. I am deeply indepted to him for introducing me to the field of climate dynamics as well as for the dedication he shows to each of his students.

We wish to thank Hai-Lin and Professor Jacques Derome for their insightful input during our bi-weekly group meetings. It is a pleasure to thank Professor John Gyakum, Eyad Atallah and David Small for their helpful comments. For all their technical help, I am grateful to Joowan Kim and Patrick Martineau.

Finally, I wish to thank my family and my close friends, especially Cedrick O'Shaughnessy and Bernard Asselin, for keeping me sane during the past 2 years as well as for our inspired discussions about life, geology, engineering and atmospheric science.

Contribution of authors

I acknowledge the contribution of my advisor, Professor Seok-Woo Son, for co-authoring the manuscript which appears in chapter 3 of this thesis. I certify that the content presented here was written by myself. Professor Son's contribution consisted of guidance towards the writing and improvement of the original content.

Abstract

The performance of the Global Environmental Multiscale (GEM) model, Canadian operational numerical model, in reproducing atmospheric low-frequency variability is first evaluated in the context of Northern Hemisphere blocking climatology. The validation is conducted by applying a comprehensive but relatively simple blocking detection algorithm. Comparison to reanalysis reveals that the maximum blocking frequency over the north Atlantic and western Europe is generally underestimated and its peak season is delayed from late winter to spring. This contrasts with the blocking frequency over the north Pacific which is generally overestimated during all seasons. The biases in blocking frequency are found to be largely associated with the biases in climatological background flow. Specifically, modelled stationary wave shows a seasonal delay in zonal wavenumber 1 and an eastward shift in zonal wavenumber 2 components. Next, we extend our methodology to preliminary analyses of Northern Hemisphere blocking climatology from a subset of climate models participating in the Coupled Model Inter-comparison Project phase 5 (CMIP5). Historical integrations reveal that the maximum Euro-Atlantic blocking frequency is generally underestimated during the cold season and that significant overestimation of maximum Pacific blocking frequency occurs throughout the year in some models, as compared to reanalysis. In contrast, RCP8.5 integrations show a weak hint of reduced blocking frequency over the Pacific sector in comparison to historical integrations. However, no significant trend in terms of block duration within the RCP8.5 integrations is found.

Résumé

Les performances du modèle Global Environment Multiscale (GEM), qui est le modèle numérique opérationel Canadien, à reproduire les variabilités atmosphériques de basse fréquence sont évaluées en premier lieu dans le contexte de la climatologie de bloquage atmosphérique dans l'hémisphère Nord. Afin de valider le modèle, un algorithme de détection de bloquage qui est à la fois compréhensif et relativement simple est appliqué aux données atmosphériques. Les résultats montrent que la fréquence maximum de bloquage au dessus de l'Atlantique Nord et l'Europe de l'Ouest est généralement sous-estimée et il y un délai dans la saison d'amplitude maximale puisqu'elle se produit au printemps au lieu de tard en hiver. De plus, la fréquence de bloquage est généralement sur-estimée au dessus du Pacifique Nord. Il a été trouvé que les erreurs dans la fréquence de bloquage sont grandement associées aux erreurs dans la circulation climatologique de l'atmosphère. En fait, les ondes stationnaires modélisées montrent un délai saisonnier dans le nombre d'onde zonal 1 et un déplacement vers l'Est des composantes du nombre d'onde zonal 2. Ayant confiance en la capacité de notre index pour identifier des bloquages atmosphériques, nous appliquons notre méthodologie sur des analyses préliminaires de bloquage climatologique dans l'hémisphère Nord à partir d'un sous-ensemble de modèles climatologiques faisant partie du Coupled Model Inter-Comparison Project Phase 5 (CMIP5). Les intégrations historiques révèlent que la fréquence maximale de bloquage sur l'Euro-Atlantique est généralement sous-estimée durant la saison froide et que la sur-estimation de la fréquence maximale de bloguage sur le Pacifique se produit tout au long de l'année dans certains modèles. En comparaison, les intégrations de type

RCP8.5 montrent un léger indice d'une réduction de la fréquence de bloquage sur le Pacifique même si aucune tendance significative en terme de durée de bloquage n'a été trouvée.

Contents

List of Figures

List of Tables

Chapter 1

Introduction

The prevailing westerly flow, in the Northern Hemisphere, occasionally becomes blocked by the occurrence of persistent synoptic scale high pressure systems commonly referred to as atmospheric blocking events (Fig. 1.1). Lasting days to weeks, a blocking high remains quasi-stationary relative to the background flow, interrupting the eastward progression of synoptic scale systems causing them to divert meridionally. These persistent high pressure systems largely occur at the ends of the climatological storm tracks over the northeastern Atlantic and Pacific basins, often inducing a split westerly jet there.

The earliest attempts at defining individual blocking events were introduced in the pioneering studies by Elliott and Smith [1949] and Rex [1950a]. Elliott and Smith [1949] used SLP anomalies to objectively define a blocking event as: "A band fifteen degrees of longitude wide and covering 55°N and 60°N latitudes must experience pressure departures of $+20mb$ or more at least three consecutive days." On the other hand, Rex [1950a] utilized the 500-hPa geopotential height field to quantify a blocking event from a set of subjective criteria as below:

- The basic westerly current must split into two branches.
- Each branch current must transport an appreciable amount of mass.
- The double-jet system must extend over at least 45° of longitude.
- A sharp transition from zonal-type flow upstream to meridional-type flow downstream must be observed across the current split.
- This pattern must persist for at least 10 days.

Recently, other indices ranging in complexity have also been proposed to define blocking on the 500-hPa geopotential height field. The two most widely used blocking indices, Dole and Gordon [1983] and Tibaldi and Molteni [1990], objectively isolate either persistent positive geopotential height anomalies or synoptic-scale meridional height reversals about a reference latitude (Fig. 1.2). Variations of these indices using different variables have also been used in the literature such as potential temperature on the dynamic tropopause [Pelly and Hoskins, 2003], potential vorticity [Schwierz et al., 2004], meridional wind [Kaas and Branstator, 1993] and stream function [Metz, 1986]. However, their underlying methodologies largely stem from the seminal work of Elliott and Smith [1949] and Rex [1950a].

The impact of atmospheric blocking on surface weather and extratropical circulation is well documented (e.g., Rex 1950b, Stein 2000, Trigo et al. 2004). Blocking highs are associated with significant temperature anomalies beneath the block as well as increased precipitation and storm activity around the block. Since blockings may persist for upwards of 10 days, they may even influence the short term climate: i.e., a small number of blockings can strongly influence the climate characteristics of a single season [Stein, 2000]. Exceptionally long-lasting blocking events can also engender significant changes in surface conditions, relevant to human society. Striking examples include the recent 2003 European and 2010 Russian heat waves, resulting from persistent blocking episodes (Fig. 1.3), both of which lead to record breaking temperatures and large increases in mortality rates in the surrounding area [Black et al., 2004, Dole et al., 2011]. The 2010 event further contributed to largescale crop damage resulting in severe economic losses [Matsueda, 2011], and has also been suggested as a culprit of catastrophic flooding in Pakistan, due to its concomitant downstream trough [Webster et al., 2011].

The above-described importance of blocking underlines the need for the reliable simulation of blocking highs in climate studies. The predictability of blocking in global climate models has been assessed by several authors (e.g., D'Andrea et al. 1998, Scaife et al. 2010). Despite strong progress in model development in recent years, it is well known that previous generations of global climate models systematically underestimate blocking frequency, especially over the North Atlantic region.

To this date, the global environment multiscale (GEM) model, canadian operational forecast model, has not been validated in the context of Northern Hemisphere blocking climatology. Similarly, validation of the present climate as simulated by the most recent generation of global climate models, coupled model inter-comparison project phase 5 (CMIP5), is also missing. Examining the ability of these models to reliably simulate blocking in the Northern

Hemisphere is the primary goal of this research. This would improve our understanding of short-term predictability of blocking in an operational model and long-term change of low-frequency variability forced under anthropogenic climate change.

It should be noted that relatively few studies have been conducted for documenting the blocking response to anthropogenic forcings in the future climate. In fact, blocking was *not* commented upon in the IPCC AR4 report (Solomon et al. 2007). Only a few recent studies have addressed this issue. Given the crucial role blocking plays in influencing mid-latitude climate and its potential for high impact weather, knowledge of changes in blocking in response to anthropogenic forcings is critical. As such, examining potential changes in blocking in future climate, as simulated by the CMIP5 models, would be of significant value.

This thesis is organized as follows. A review of the dynamics and energetics relevant to atmospheric blocking are first presented in chapter 2. It is followed in chapter 3 by an evaluation of the Northern Hemisphere blocking climatology in the GEM model. Geographical distribution, seasonal cycle and statistics of individual blocking events are quantitatively compared with those derived from the NCEP-NCAR Reanalysis. This comparison is particularly conducted by applying a newly developed blocking index, which is relatively simple but still comprehensive, to the GEM and NNR data in a same resolution. Chapter 4 presents a preliminary analysis of Northern Hemisphere blocking climatology in the current and future climate as simulated by the CMIP5 models. The ability of the CMIP5 models to reliably simulate Northern-Hemisphere blocking in the current climate is used to measure the confidence within which they are able to faithfully reproduce changes in a warming climate. Lastly, a summary and conclusions are given in chapter 5.

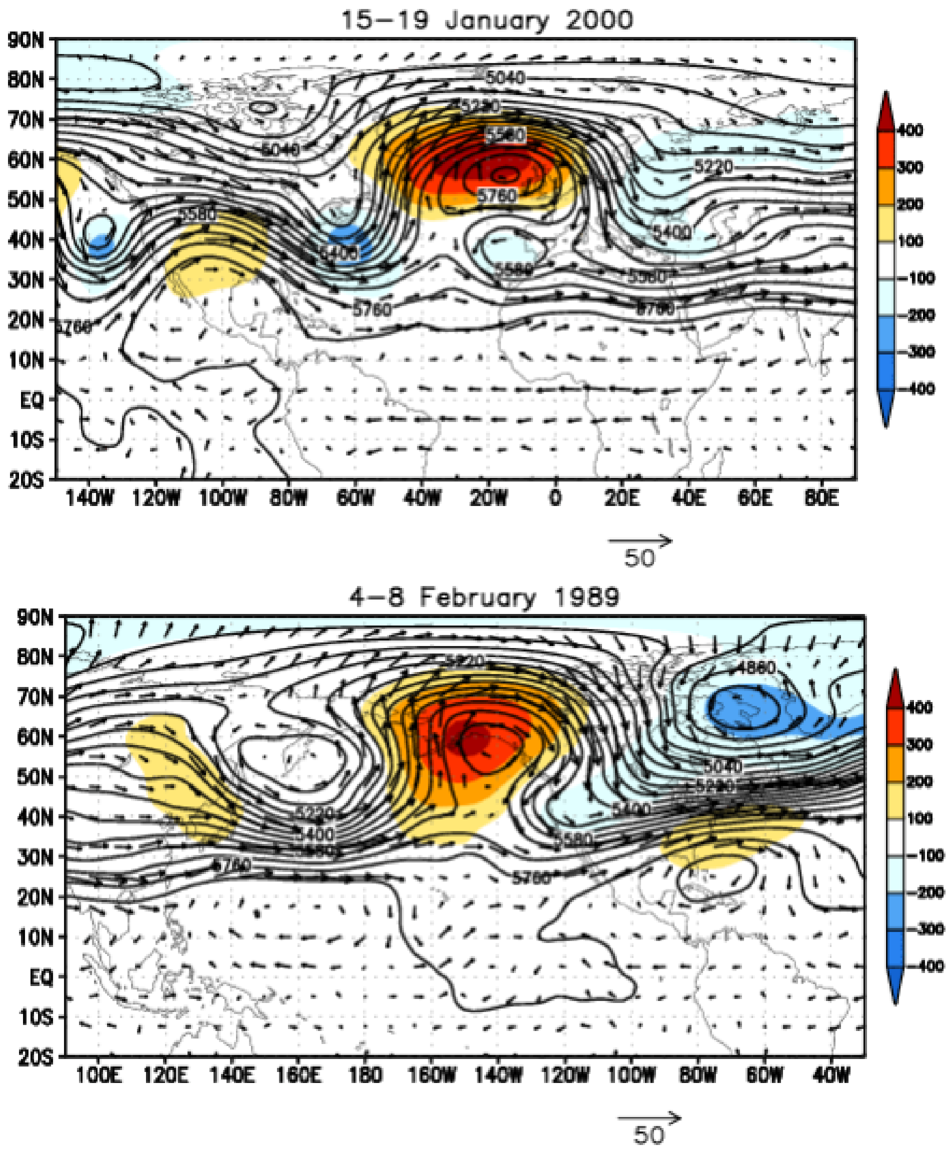

Figure 1.1: Illustrative examples of the two canonical types of blocking events: (Top) dipole type blocking event characterized by a high over low-pressure pattern. (Bottom) omega type blocking event characterized by two low-pressure systems digging into a high pressure ridge. Contours (shading) represent 500-hPa geopotential height (anomalies) and vectors denote streamfunction. Contour interval $60m$. Taken from http://www.cpc.ncep.noaa.gov/products/precip/CWlink/blocking.

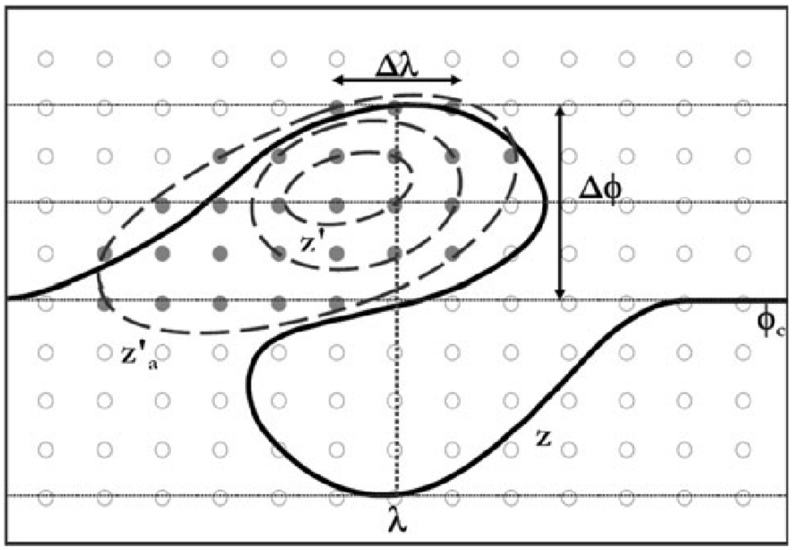

Figure 1.2: Illustrative example of the Tibaldi and Molteni and Dole and Gordon blocking index types using a schematic diagram of a block centered at λ. Solid lines (dashed lines) represent the total (anomaly) height field z (z') during a blocking episode. ϕ_c represents the reference latitude from which the geopotential height gradient is calculated at λ. $\Delta\lambda$ and $\Delta\phi$ represent the typical zonal and meridional scales of the block. Filled dots reflect the grid points satisfying the anomaly threshold z'_a. Taken from Fig. 2 of Barriopedro et al. [2010a].

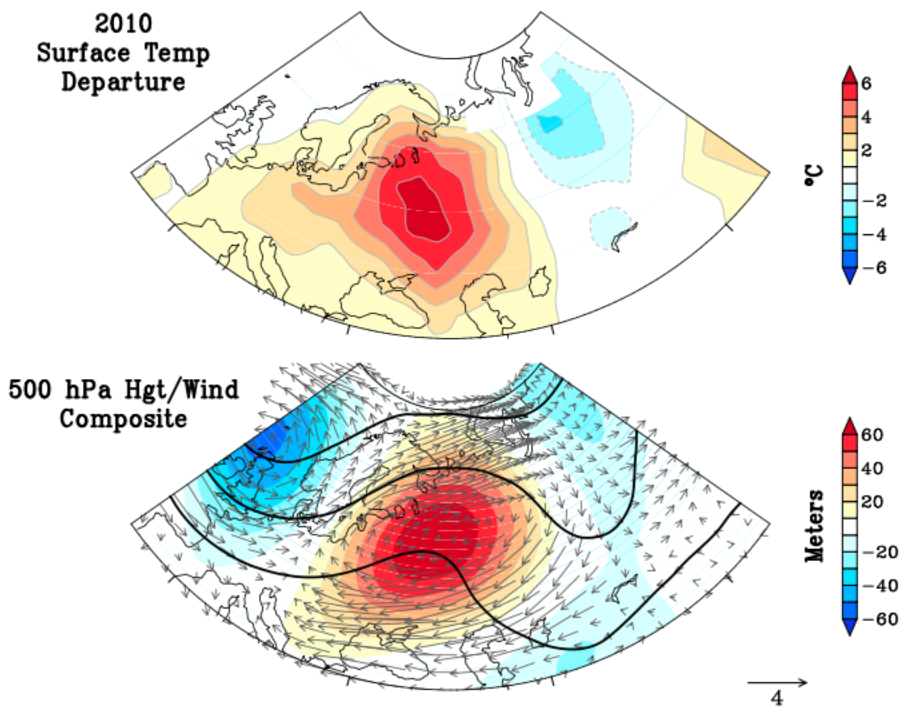

Figure 1.3: Observed climate conditions for July 2010 over western Russia. (Bottom) NCEP/NCAR Reanalysis monthly mean 500-hPa geopotential height (contour interval: $100m$), anomalies (shading) and wind vector anomalies (arrows, ms^{-1}) for July 2010. Anomalies are relative to the 1948-2009 climatology. (Top) Observed surface air temperature anomalies for July 2010 (base period is 1880-2009) from NOAA merged land air and sea surface temperature data set. Taken from Fig. 2 of Dole et al. [2011].

Chapter 2

Review of the dynamics and energetics relevant to atmospheric blocking events

2.1 Dynamics

Despite the importance of blocking for high impact weather and mid-latitude climate, there is no consistent theory for blocking onset, maintenance and dissipation as of yet. One of the earliest proposed dynamical mechanisms, the hydraulic jump, was used by Rex [1950b] to explain the sharp transition from a strong westerly jet upstream to a weak flow downstream of a blocking high. This mechanism was however opposed by Egger [1978], based on the argument that the stability of a blocking high cannot be associated with the turbulence involved with a hydraulic jump. A number of recent theoretical approaches have been suggested since, and can be largely classified into two broad categories: *global processes* wherein blocking is examined in the context of planetary scale processes and *local processes* wherein blockings are considered spatially isolated phenomenon endemic to the exit regions of the Atlantic and Pacific storm tracks. To better understand blocking, the major dynamical theories relevant to blocking are briefly reviewed in this section.

The role of global-scale processes has been emphasized in the studies of Charney and Devore [1979] and Tung and Lindzen [1979] who suggested that blocking can be generated from the resonant amplification of planetary-scale waves to stationary forcings such as land-sea thermal contrast and orography. Specifically, Tung and Lindzen [1979] showed that planetary waves can become resonant and produce a blocking-like structure when the background flow is such that the phase speed of the wave reduces to zero. Blocking has also been suggested to occur as a result of the resonant interaction of planetary scale waves [Colucci et al., 1981, Egger, 1978] or the interference of stationary planetary waves [Austin, 1980]. These theoretical approaches are consistent with enhanced planetary-scale wave energy and planetary-scale flow during blocking periods [Hansen and Sutera, 1984, 1993]. It should be noted, however, that stationary forcings crucial to some of the mechanisms in the aforementioned studies are not a necessary condition for blocking formation. For instance, Hu et al. [2008] have shown that blocking can occur in aqua planet simulations, in the absence of topography or land-sea thermal contrast, resulting from the interaction of quasi-stationary Rossby waves and baroclinic eddies.

In contrast to global scale processes, a number of blocking studies emphasize the local role of high-frequency transient eddy forcing in the onset and maintenance of blocking. The connection between high-frequency eddies and blocking was first brought forward in the synoptic study by Berggren et al. [1949] and was further corroborated in the case study by Green [1977]. Green [1977] suggested that the 1976 European blocking episode, located near the end of the Atlantic storm track, was maintained by transient eddy vorticity fluxes from upstream synoptic scale eddies. This process was subsequently examined in the seminal modelling work of Shutts [1983], establishing the so-called barotropic eddy-straining mechanism. Shutts [1983] argued that the deformation field of a blocking flow can organize high-frequency eddies such that it can be maintained by them through upscale enstrophy cascade and poleward advection of anticyclonic vorticity (Fig. 2.1). This mechanism gained additional support from ensuing diagnostic studies [Illari, 1984, Mullen, 1987].

Recently, Nakamura et al. [1997] have attempted to isolate the relative roles of high and low-frequency dynamics in blocking formation over the Atlantic and Pacific basins. Composite time evolutions of strong blocking events show the feedback from high-frequency eddies accounting for more than 75% and less than 45% of the maintenance of Pacific and Atlantic blocking, respectively. Cash and Lee [2000] used a more complete vorticity budget than Nakamura et al. [1997] to examine the time evolution of composite Atlantic blockings showing that high and low-frequency non-linear interactions contribute equally towards the maintenance of Atlantic blockings. Their results, however, suggest that time averaged budgets used in previous diagnostic studies (e.g., Illari 1984, Mullen 1987) exaggerate the importance of high-frequency eddies in the maintenance of blocking.

Blocking may also be examined from the local perspective of a breaking synoptic-scale Rossby wave. Pelly and Hoskins [2003] developed a blocking index based on the synoptic-scale reversal of potential temperature on the dynamic tropopause, intrinsically associating blocking with the physical process of a breaking Rossby wave. As such, it should be noted that not all Rossby wave breakings are associated with blockings [Berrisford et al., 2007] and that not all blockings are associated with breaking Rossby waves [Altenhoff et al., 2008]. The blocks that are associated with Rossby waves, however, are primarily located in regions of strong deformation near the end of Atlantic and Pacific storm tracks [Pelly and Hoskins, 2003, Tyrlis and Hoskins, 2008].

The use of the PV framework to consider breaking synoptic-scale Rossby waves as blockings has important dynamical considerations. As discussed in Altenhoff et al. [2008], the background PV distribution in the upper troposphere can be redistributed through wave breaking such that resulting anomalies can create a viable blocking pattern. Specifically, combinations of a low PV anomaly poleward of the jet and high PV anomalies equatorward of the jet can effectively generate a circulation capable of counteracting the background flow, ensuring the stationarity of the block (Fig. 2.2). Isentropic advection of subtropical low-PV air by the equatorward anomaly can also act to reinforce the blocking pattern, enhancing its persistence. The resulting PV configuration may be further maintained in a manner similar to the eddy straining as discussed in Shutts [1983], where upstream eddies are stretched meridonally, depositing low (high) PV on the poleward (equatorward) side of the block [Pelly and Hoskins, 2003].

2.2 Low-frequency energetics and blocking

It is well known that blocking contributes towards a significant portion of the mid-latitude atmospheric low-frequency variability. This has motivated researchers to examine dynamical processes of blocking formation and maintenance using low-frequency energetics over limited regions and the globe. Not all low-frequency activities, however, are associated with blockings. This limits quantitative application of energetics to blocking studies. Nonetheless, low-frequency energetics are still helpful to diagnose and understand the relative importance of non-linear eddy-eddy interaction and eddy-mean flow interaction in the formation and maintenance of blocking. To better understand blocking, the energetics of low-frequency eddies (and blocking) and their relation to the time-mean flow are briefly reviewed in this section.

A number of studies have shown distinctively different properties between transient eddies with timescales larger than 10 days (low-frequency eddies in this thesis) and eddies with shorter timescales (high-frequency eddies) (e.g., Hoskins et al. 1983). For instance, distributions of **E**-vectors, as defined by Hoskins et al. [1983], show markedly different anisotropy, wave propagation and interaction with the mean-flow depending on their frequency bands (Fig. 2.3). The distinction between eddy timescales is further manifested in their maintenance. High-frequency eddies are largely maintained through the classical *baroclinic* conversion of time-mean available potential energy (APE) to transient synoptic scale kinetic energy (KE). In contrast, *barotropic* instability of the longitudinally dependent background flow plays an important role in maintaining low-frequency eddies. Simmons et al. [1983] found that the most rapidly growing modes in their barotropic model simulation, where subtropical and tropical thermal forcings are imposed in realistic background flow, resembled the Pacific/North American and East Atlantic teleconnection patterns which are the leading low-frequency variabilities in the NH. Wallace and Lau [1985] later examined this process using observational data sets, finding that low-frequency eddies tend to extract KE from the wintertime mean flow, in agreement with Simmons et al. [1983].

Needless to say, barotropic energy conversion is not the only energy source of low-frequency eddies. Using observational and modelling data sets, Sheng and Hayashi [1990a,b] showed that the baroclinic conversion of time-mean APE to transient KE plays a major role in the annual-mean hemispherically-integrated energetics of low-frequency disturbances. A significant amount of KE transferred to low-frequency eddies was also reported from non-linear interactions with high-frequency eddies. The slight discrepancy between Simmons et al. [1983] and Sheng and Hayashi [1990a,b] was adressed by Sheng and Derome [1991a,b] by considering the geographical distribution of the energetics terms in both winter and summer. Hemispherically integrated results showed the barotropic energy conversion of low-frequency eddies changes sign from winter to summer, possibly explaining why barotropic processes are relatively weak in the annual mean energetics reported in Sheng and Hayashi [1990a,b]. Further investigation revealed significant longitudinal variations in the general circulation statistics. Both regions of maximum barotropic energy conversion from the background flow to low-frequency eddies and non-linear energy transfer from high frequency eddies to the low-frequency eddies are collocated with regions of maximum low-frequency KE, typically over the eastern Atlantic and Pacific basins. These results support those of Simmons et al. [1983] and Wallace and Lau [1985] while reconciling those of Sheng and Hayashi [1990a,b] and indicate that over the oceans, low-frequency disturbances are primarily forced by transient baroclinic waves and maintained by a barotropically unstable background flow.

The barotropic energy conversion, shown in Simmons et al. [1983], is briefly discussed below to illustrate the mechanism of how the time-mean flow can affect low-frequency eddies and blocking. The barotropic energy conversion from the time-mean flow to transient eddies, BTC, is given by:

$$BTC = -(\overline{u'^2} - \overline{v'^2}) \left[\frac{1}{a\cos\phi} \frac{\partial \bar{u}}{\partial \lambda} - \bar{v} \frac{\tan\phi}{a} \right] - (\overline{u'v'}) \left[\frac{\cos\phi}{a} \frac{\partial}{\partial \phi} \left(\frac{\bar{u}}{\cos\phi} \right) + \frac{1}{\cos\phi} \frac{\partial \bar{v}}{\partial \lambda} \right] \tag{2.1}$$

where u and v are the zonal and meridional wind components respectively, overbars represent a time average, primes denote deviations from the time mean, λ is the longitude, ϕ is the latitude and a is the radius of the earth [Simmons et al., 1983]. It is shown by Simmons et al. [1983] that this equation can be simplified in the mid-latitudes to a good approximation to the form:

$$BTC = \mathbf{E} \cdot \nabla \bar{u} = BTC_x + BTC_y \tag{2.2}$$

where the $\mathbf{E}$ vector is defined as in Hoskins et al. [1983] as:

$$\mathbf{E} = -(\overline{u'^2} - \overline{v'^2}, \overline{u'v'}) \tag{2.3}$$

and

$$\nabla \bar{u} = \left(\frac{1}{a\cos\psi} \frac{\partial \bar{u}}{\partial \lambda}, \frac{1}{a} \frac{\partial \bar{u}}{\partial \psi} \right) \tag{2.4}$$

The first term on the right hand side describes energy transfer due to anisotropy of the disturbances and zonally-varying background flow. Transient eddies extract KE from the mean flow when zonally elongated eddies ($\overline{u'^2} > \overline{v'^2}$, westward pointing **E**-vectors) occur in the region of diffluence ($\partial\bar{u}/\partial\lambda < 0$) (Fig 2.4). This contrasts with the second term on the right hand side that is the classical BTC from the zonally uniform flow to the eddies by an upgradient eddy momentum flux.

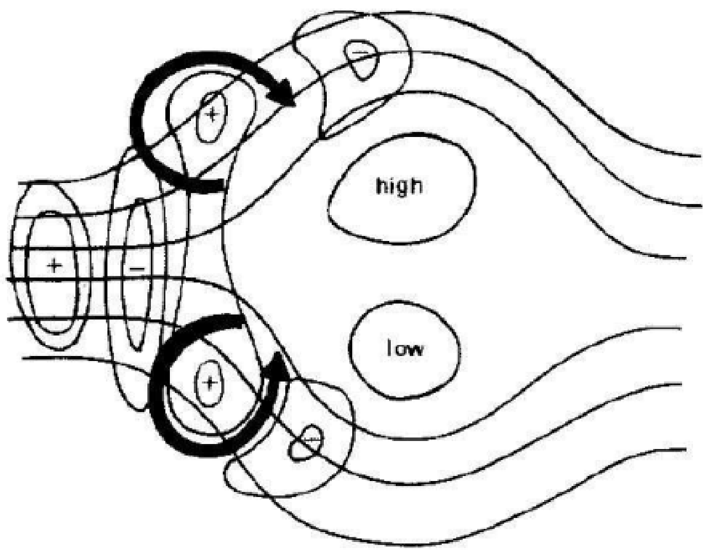

Figure 2.1: Schematic of the deformation of high-frequency eddies propagating into a split jet stream together with their associated vorticity forcing pattern. Taken from Fig. 1 of Shutts [1983]

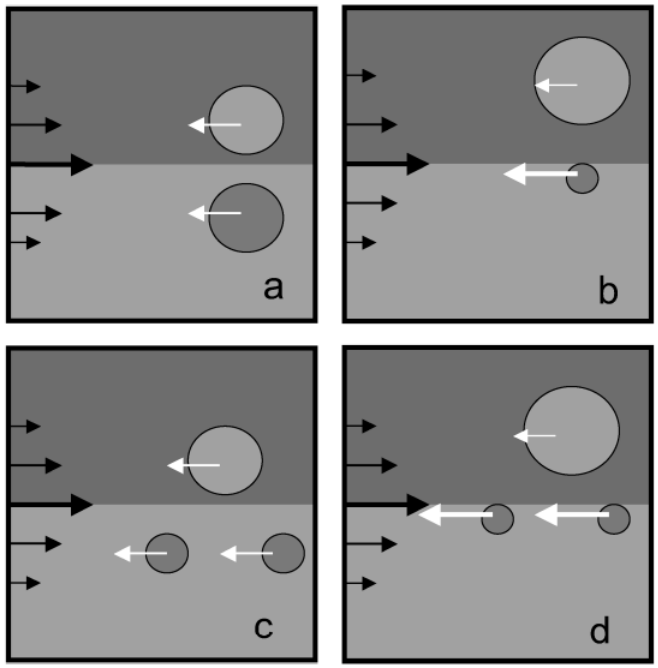

Figure 2.2: Schematic of four idealized PV configurations on an isentropic surface possibly linked to blocking. In each panel, the background PV distribution corresponds to a pattern of uniformly high (low) PV located polewards (equatorwards) of a zonally aligned interface, and the circular anomalies correspond to a redistribution of the background PV. The black and white arrows indicate, respectively, the jet accompanying the background PV distribution and the perturbed flow attributable to the PV anomalies. The top and bottom panels resemble dipole and omega type blocking, respectively. Taken from Fig. 2 of Altenhoff et al. [2008]

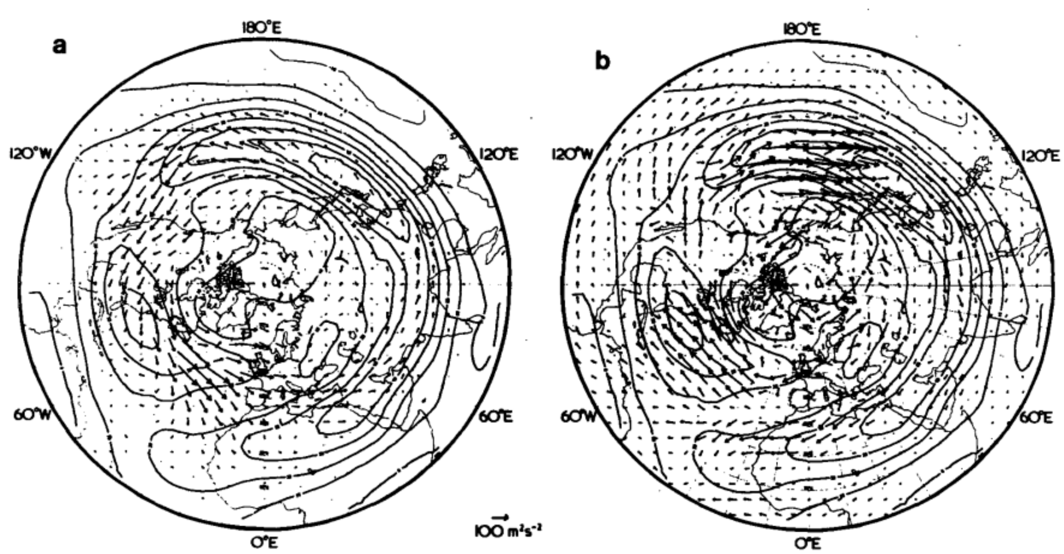

Figure 2.3: Northern Hemisphere ECMWF 1979-1980 winter 250 hPa **E**-vectors superimposed over the mean zonal wind for: (a) high-frequency eddies and (b) low-frequency eddies. Contour interval is 10 ms^{-1}. Taken from Fig. 6 of Hoskins et al. [1983].

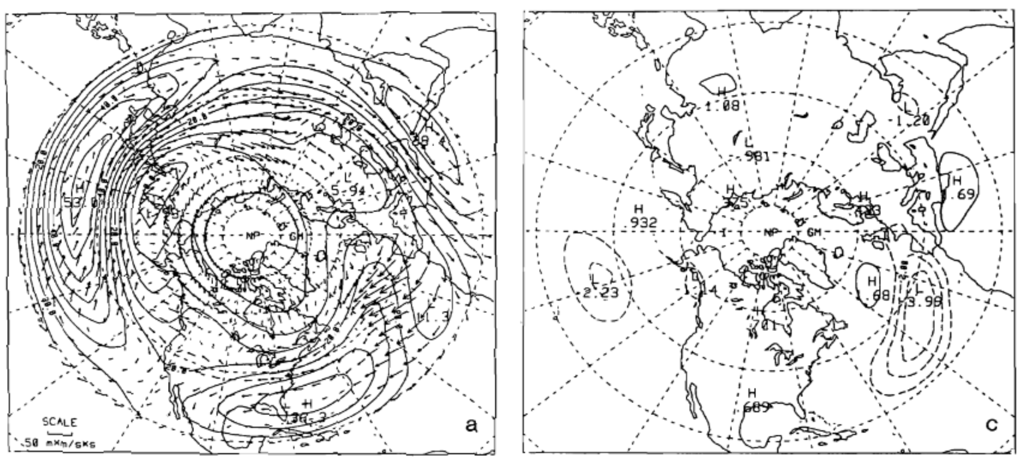

Figure 2.4: The Canadian Climate Centre (CCC) GCM winter 300 hPa (a) low-frequency **E**-vectors superimposed over the climatological zonal wind and (b) BTC from the time-mean flow to low-frequency eddies due to anisotropy of the disturbances ($\overline{u'^2} > \overline{v'^2}$) and zonally-varying background flow ($\partial\bar{u}/\partial\lambda < 0$). Contour interval in (a) is 5 ms^{-1} and 10^{-4}Wkg^{-1} in (b). Taken from Fig. 6a,c of Sheng and Derome [1991b].

Chapter 3

Evaluation of Northern Hemisphere blocking climatology in the Global Environment Multiscale (GEM) model

In this chapter we evaluate the performance of the Global Environmental Multiscale (GEM) model, Canadian operational numerical model, in reproducing Northern Hemisphere blocking climatology using a newly defined blocking index. The results obtained in this chapter provides confidence in the blocking index and forms the basis of the methodology used in chapter 4.

Abstract

The performance of the Global Environmental Multiscale (GEM) model, Canadian operational numerical model, in reproducing atmospheric low-frequency variability is evaluated in the context of Northern Hemisphere blocking climatology. The validation is conducted by applying a comprehensive but relatively simple blocking detection algorithm to a 20-year (1987-2006) integration of the GEM model in climate mode. The comparison to reanalysis reveals that, although the model can reproduce Northern Hemisphere blocking climatology reasonably well, the maximum blocking frequency over the north Atlantic and western Europe is generally underestimated and its peak season is delayed from late winter to spring. This contrasts with the blocking frequency over the north Pacific which is generally overestimated during all seasons. These misrepresentations of blocking climatology are found to be largely associated with the biases in climatological background flow. Modelled stationary wave shows a seasonal delay in zonal wavenumber 1 and an eastward shift in zonal wavenumber 2 components. High-frequency eddies are however consistently underestimated both in the north Atlantic and Pacific, indicating that the biases in eddy fields might not directly contribute to the blocking biases, particularly in the north Pacific.

3.1 Introduction

Atmospheric blocking is one of the most striking features of extratropical low-frequency variability. A synoptic-scale high pressure system, often accompanied by low pressure system at lower latitudes, occasionally becomes quasi-stationary for several days to a few weeks against the background flow. This quasi-stationary system, referred to as a block, interrupts the eastward propagation of synoptic disturbances by reversing the climatological zonal flow.

As a blocking high is quasi-stationary by nature, it has a significant impact on surface temperature and precipitation [Rex, 1950a, Trigo et al., 2004]. A dramatic example is the 2010 Russian heat wave that resulted from a blocking episode that persisted for over a month [Dole et al., 2011]. This event is associated with over 15,000 deaths in Russia and severe economic losses in neighbouring countries through crop damage [Matsueda, 2011]. The resulting downstream trough has also been suggested as a possible culprit of Pakistan flooding in 2010 [Webster et al., 2011].

The impact of blocking is not limited to the surrounding regions of a blocking high. It is known that long-lasting blocking events are often associated with extratropical teleconnection patterns [Croci-Maspoli et al., 2007a, Renwick and Wallace, 1996, Woollings et al., 2008]. In the Northern Hemisphere (NH), the two preferred regions of blocking occurrence are the Europe-northeastern Atlantic (hereafter EA blocking) and the north Pacific (PA blocking). These regions coincide with the preferable locations of two leading teleconnection patterns in the NH: namely the North Atlantic Oscillation (NAO) and the Pacific North American (PNA) pattern. It is hence not surprising to find that, EA blocking events are often concurrent with the negative phase of the NAO [Croci-Maspoli et al., 2007a, Woollings et al., 2008] whereas PA blocking events are often associated with the negative phase of the PNA, although the causal relationship is unclear. Recent studies further showed that NH blocking events could even affect the stratospheric circulation. Martius et al. [2009] demonstrated that long-lasting blocks could excite planetary-scale waves that propagate into the stratosphere and break at the polar vortex during the cold season, causing the so-called sudden stratospheric warming. Woollings et al. [2010] proposed that there might be a two-way interaction between stratospheric circulation and tropospheric blockings.

The importance of blocking highs on local and remote weather systems has increased the need for the reliable simulation of blocking events in climate models. It is however known that blocking frequency is generally underestimated in the current generation of climate models [D'Andrea et al., 1998, Scaife et al., 2010]. This failure has been often attributed to the model resolution. The poleward advection of anticyclonic vorticity and upscale entrophy cascade by high frequency transient eddies is widely recognized as an important mechanism for blocking maintenance [Mullen, 1987, Nakamura et al., 1997, Shutts, 1983]. It follows that if high-frequency eddy activity is underestimated by model resolution, it could lead to rather weak eddy forcing and subsequently less frequent blocking events. This resolution issue is well documented for EA blockings [Matsueda et al., 2009, Ringer et al., 2006, Tibaldi et al., 1997]. The corresponding effect on PA blockings, however, is not quite clear, suggesting that PA blocking is likely affected by other dynamical processes as well [Tibaldi et al., 1997]. Matsueda et al. [2009] in fact showed that PA blocking could be significantly overestimated in high-resolution model simulations.

It is known that not only transient eddies but also the time-mean flow is important in simulating NH blockings. The influence of the time mean flow, especially the location of the westerly jet, on the formation of blocking was explicitly discussed in Kaas and Branstator [1993] who forced their GCM towards a zonal mean state representing suppressed or enhanced blocking activity. As anticipated, they found more frequent blocking events with the mean state associated with enhanced blocking activity, that is, relatively strong zonal winds around 30°N and weak winds around 50-60°N. In accordance with this finding, Barnes and Hartmann [2010] found a robust reduction in EA blocking frequency with the poleward shift of the Atlantic eddy-driven jet in Coupled Model Inter-comparison Project phase 3 (CMIP3) scenario integrations.

In regards to the shape and intensity of the jet, it has also been shown that excessive zonality and the underestimation of stationary wave could be an important error source in model simulations of blocking [Barriopedro et al., 2010a, Doblas-Reyes et al., 2002]. Excessive westerlies may result from anomalous momentum transfer from synoptic-scale eddies to the mean flow, decreasing the frequency of large-scale ridges over blocking regions [Doblas-Reyes et al., 2002, Wallace and Hsu, 1985]. In the diagnostic study by Cash and Lee [2000], linear interactions between low-frequency eddies and the time-mean flow are shown to dominate the vorticity budget during the onset and decay of modelled EA blocking. Their results suggest that systematic model biases in background flow could affect the role of those interactions by modifying the background meridional potential vorticity gradient.

The importance of the background flow is further consistent with theoretical approaches that consider blocking as the result of wave-wave interactions such as the interference or resonant interaction of planetary-scale waves [Austin, 1980, Colucci et al., 1981, Egger, 1978] or the interaction of transient eddies and quasi-stationary planetary-scale waves [Cash and Lee, 2000, Colucci, 1985, Hu et al., 2008, Nakamura et al., 1997]. It follows that weaker planetary-scale wave activity in the model could result in weaker interactions between waves, causing less frequent blocking events in the model [Barriopedro et al., 2010a, Doblas-Reyes et al., 2002].

The model biases in blocking climatology may result from multiple factors instead of a single factor. In fact its is often difficult to identify the exact reason of model biases as individual factors (e.g., high-frequency eddies, time-mean flow etc.) are interacting with each other. The evaluation of numerical models in the context of blocking climatology is however still helpful for quantitative understanding of model performance and possible attribution of model biases. This is particularly true for operational models as blocking is one of the most important low-frequency variability in the extratropics which has a significant impact on surface weather.

Extending previous studies, this study examines NH blocking climatology in an operational model. Specifically, the Canadian operational model, Global Environment Multiscale (GEM) model, is evaluated by applying a newly developed blocking index to the long-term model output. The blocking index employed in this study differs from traditional ones as it combines the two most commonly-used blocking indices. Since it combines advantages of the two indices, it is more comprehensive than each index but still relatively simple. This index is applied to both the reanalysis and model output to objectively characterize blocking climatology. The possible sources of blocking biases are then discussed by examining blocking statistics, stationary wave, transient eddies and energetics. Although this type of study, model validation in the context of blocking climatology, is not new, the identified blocking bias in the model turns out somewhat different from the one typically documented in the literature. It is found that blocking frequency over North Pacific is overestimated in most seasons even if the model is integrated with relatively coarse resolution. This contrasts with EA blocking whose frequency is either overestimated or underestimated depending on the season.

This chapter is organized as follows. The data used in this study are briefly described in section 2. Section 3 presents the motivation and details of our blocking index. It is followed by 50-year climatology of the reanalysis data. The blocking simulated by the model is then evaluated in section 5 by comparing a 20-year blocking climatology with reanalysis data for the same time period. The possible sources of blocking biases are discussed in section 6 with an emphasis on the bias in time-mean flow.

3.2 Data

The reference blocking climatology is constructed from the National Centers for Environmental Prediction (NCEP)-National Center for Atmospheric Research (NCAR) Reanalysis data (NNR, Kalnay et al. [1996]). The 50-year dataset, extending from 1960 to 2009, is used to generate a long-term climatology, and to validate the blocking index employed in this study.

The model evaluated in this study is the GEM model of Recherche en Prévision Numérique, Environment Canada [Côte et al., 1998a,b]. It is an operational forecast model at the Canadian Meteorological Centre, and is integrated in climate mode by using the version 3.2.2 at a horizontal resolution of 2° latitude by 2° longitude with 50 vertical levels (the model top at 5 hPa). The model was initialized at 00Z of January 1, 1985, and integrated for 22 years by prescribing surface boundary conditions from the Seasonal Prediction Model Intercomparison Project-2 (SMIP-2) boundary data. After discarding first two years of spin-up period, 20 years of data, from 1987 to 2006, are analyzed. All daily mean data are first interpolated into 2.5° latitude by 2.5° longitude resolution to be consistent with the NNR resolution. Blocking statistics and the related analyses are then performed using this interpolated data, and the results are directly compared with those derived from the NNR over the same time period.

3.3 Methodology

3.3.1 Background

As recently reviewed by Barriopedro et al. [2010b], a variety of blocking indices, differing in variables and ranging in complexity, have been used in the literature. The two most widely-used blocking indices, those proposed by Dole and Gordon [1983] and Tibaldi and Molteni [1990], are based on the 500-hPa geopotential height field. Other blocking indices use potential vorticity [Schwierz et al., 2004], stream function [Metz, 1986], potential temperature on the dynamic tropopause [Pelly and Hoskins, 2003] or meridional wind [Kaas and Branstator, 1993]. These indices also differ in the use of absolute or anomaly fields.

At present, there is no consensus on a standard or universal blocking index. This disagreement in blocking index, which is essentially caused by the different definition of blocking itself, has limited comprehensive understanding of atmospheric blocking. It is hence helpful to critically review salient features of traditional blocking indices to better identify blocking highs. Below, the two most widely-used blocking indices applied to the 500-hPa geopotential height field and other recent approaches are briefly re-visited.

The so-called Dole-Gordon index [Dole and Gordon, 1983] identifies atmospheric blocking as a persistent positive geopotential height anomaly at 500 hPa. This index provides blocking statistics on the latitude-longitude domain in a relatively simple way. It however suffers from arbitrary blocking anomaly thresholds and the need of a robust climatology to define anomalies [Doblas-Reyes et al., 2002]. More importantly this approach does not necessarily detect blocking highs because persistent anomalies can be associated with weak troughs, subtropical highs or sub-polar highs which do not really block the westerly flow [Liu, 1994]. In spite of refinements to the Dole-Gordon index, such as more severe threshold values (e.g., Sausen et al. 1995) or defining anomalies relative to a sector mean (e.g., Mullen 1987), the possible misrepresentation still remains.

The Tibaldi-Molteni index, first introduced by Lejenas and Okland [1983] and subsequently modified by Tibaldi and Molteni [1990], is based on the reversal of the meridional gradient of 500-hPa geopotential height about a reference latitude. This index uses an absolute field, and does not suffer from thresholds for blocking anomalies. As it simply measures a local gradient about a reference latitude, it can be easily applied to any data set from operational weather forecasts to climate simulations. However the reference latitude, which prescribes the possible latitudinal locations of blocking highs, limits the detailed characterization of blocking highs (e.g., exact latitudinal location, blocking events outside of the reference regions, etc). This also hampers its application to different climate states in which preferable regions of blocking could change [Doblas-Reyes et al., 2002]. These issues have been partially addressed in recent studies where the Tibaldi-Molteni index is modified to use a longitudinally-varying reference latitude or a range of latitudes (e.g., Diao et al. 2006, Scherrer et al. 2006). Despite these modifications, it retains its fundamental deficiency in identifying omega or immature blocks which are not necessarily accompanied by the reversal of the meridional gradient over a given longitudinal range [Doblas-Reyes et al., 2002].

In the recent studies, blocking has also been examined using dynamical variables, such as potential temperature and potential vorticity in the upper troposphere or tropopause level, instead of the traditional 500-hPa geopotential height field. For instance, Pelly and Hoskins [2003] defined blocking as the reversal of the meridional gradient of potential temperature on the dynamic tropopause. Schwierz et al. [2004] used the potential vorticity anomalies integrated from 500 to 150 hPa. Alternatively, Kaas and Branstator [1993] and Cash and Lee [2000] identified blocking highs using meridional wind at 500 hPa within a region of northerly (southerly) wind upstream (downstream) at a given magnitude. These approaches are advantageous as the use of dynamical variables allows for the simultaneous identification of the regions of anomalous high pressure and strong anticyclonic circulation interrupting westerly flow. They, however, still suffer from traditional limitations such as the thresholds of the blocking anomalies and the reference latitude. The possible integration of stratospheric PV, which is not associated with blocking anomalies, is a further limiting factor in Schwierz et al. [2004].

3.3.2 A hybrid index

Barriopedro et al. [2010b] recently proposed a hybrid index by combining the Dole-Gordon and Tibaldi-Molteni indices. They first identified blocking highs by applying the Tibaldi-Molteni type index to the 500-hPa geopotential height field, and then searched for blocking anomalies around each blocked longitude as in the Dole-Gordon type index. This is essentially an extension of a 1-D blocking index (e.g., blocking frequency as a function of longitude only) to a 2-D index (e.g., blocking frequency as a function of latitude and longitude). While it better characterizes extratropical blocking highs, this index suffers from an inherently complex algorithm and a reliance on the prescribed blocking latitude.

In this study, we take a similar approach to Barriopedro et al. [2010b] but apply the Dole-Gordon index first. In other words, a contiguous area of blocking anomalies is identified from 500-hPa geopotential height field, and then the reversal of the meridional gradient of geopotential height is evaluated about the blocking anomaly maximum. This allows us to reduce the erroneous classification of blocking by concisely implementing the meridional height reversal. In addition, the reference latitude is absent although the blocking anomaly thresholds still remain to be specified. As described below, this approach is relatively simple but more comprehensive than the traditional algorithms and can be easily applied to large data sets especially for climatological studies.

As in Barriopedro et al. [2010b], we apply our blocking index to the 500-

hPa geopotential height field. The mid-tropospheric variable is useful to detect quasi-barotropic systems. It also allows us to directly compare the findings of the present study to previous results in the literature. This choice of 500-hPa geopotential height field however differs from the recent approaches that use upper-tropospheric dynamical variables which effectively detect baroclinic systems as well. While the choice of variable is still in debate and would vary depending on the purpose, Barnes et al. [2011] recently showed that most blocking events with significant amplitude and substantial spatial scale are reasonably well detected in all variables.

Anomalies

The geopotential height field anomaly, Z', is defined as in Sausen et al. [1995]:

$$Z' = Z - \bar{Z} - \hat{Z} \tag{3.1}$$

where Z is 500-hPa geopotential height normalized by the sine of latitude, $\bar{Z}$ is a running annual-mean of Z centered on a given day, $\hat{Z}$ is a mean seasonal cycle derived from Z^* which is a running-monthly mean of Z - $\bar{Z}$ centered on a given day (see Sausen et al. [1995] for further details). This treatment effectively removes the seasonal cycle and long-term variability of the background field. Note that, unlike in Sausen et al. [1995], the geopotential height field is normalized by the sine of latitude, taking the latitudinal variation of the Coriolis parameter into account [Dole and Gordon, 1983]. As such Z' can be directly related with eddy streamfunction at 500 hPa.

Detection

The identification and tracking algorithms of blocking highs used in this study are very similar to those in Schwierz et al. [2004]. The key difference is the additional constraint for the meridional gradient reversal.

1. Blocking anomalies are first identified by the closed contours satisfying the minimum amplitude *(A)* and spatial scale *(S)*. This isolates only strong high pressure systems in synoptic scale.

2. The blocking anomalies are then tracked in time, ensuring a sufficient overlap in blocking areas *(O)* within two days. It leaves only quasi-stationary systems.

3. The reversal of the meridional gradient of absolute geopotential height is tested around the blocking anomalies. The height gradient is simply defined as the maximum difference of the two grid points separated by $\Delta\phi$ on the equatorward side of the blocking anomaly maximum:

$$Gr(i) = max[z(i, j^*) - z(i, j^* - \Delta\phi)] \qquad j - \Delta\phi/2 \leq j^* \leq j + \Delta\phi/2 \quad (3.2)$$

   where z, i and j, respectively, denote 500-hPa geopotential height, the longitudinal and latitudinal locations of the anomaly maximum. The reversal is satisfied when:

$$Gr(i^*) < 0 \qquad i - \Delta\lambda/2 \leq i^* \leq i + \Delta\lambda/2 \qquad (3.3)$$

   at any longitudes within a range of $\Delta\phi$ longitudes centered about the anomaly maximum. This removes quasi-stationary ridges which do not block the zonal flow, but retains omega-shaped blocking with a weak local gradient reversal.

4. Finally, if the above three conditions are satisfied for a consecutive period of days *(D)*, the anomaly is labelled as a blocking event.

Criteria

The threshold values used in this study are listed below:

1. The anomaly threshold *(A)* is set to 1.5 standard deviation of geopotential height anomalies over 30°-90°N for a 3-month period centered at a given month.
2. The spatial-scale threshold *(S)* is set to $2.5\text{x}10^6$ km^2.
3. The overlap threshold *(O)* is 50% of area overlap in two days.
4. The duration criteria *(D)* is set to 5 consecutive days.
5. The meridional $\Delta\phi$ and zonal $\Delta\lambda$ scales are set to 15 degrees in latitude and 10 degrees in longitude, respectively.

Among the above criteria, the blocking index is known to be particularly sensitive to the anomaly threshold value, *(A)*. In this study, we follow the standard deviation approach as in Barriopedro et al. [2010b] but with a stricter threshold of 1.5 standard deviation. This filters out relatively weak or immature blocking highs. The 1.5 standard deviation threshold further yields a seasonal cycle of NH blocking frequency in better qualitative agreement with the seasonal cycle of low-frequency (periods of 10-90 days) eddies in comparison to the seasonal cycles obtained using lower threshold values (not shown).

The remaining criteria have received only slight modifications but are generally similar to the values proposed by Schwierz et al. [2004] and Barriopedro et al. [2010b]. These thresholds are less arbitrary since they largely depend on the typical scales of synoptic weather systems. Moreover, sensitivity tests have shown that the index is robust to changes in these thresholds (see appendix Figs. A.1-A.7).

Impact of the height gradient reversal

As described above, a key difference between the current blocking index and the traditional Dole-Gordon type indices is the additional constraint of the height gradient reversal. The impact of this additional constraint is briefly described in this section. Figure 3.1a presents the 50-year climatology of the annual-mean blocking frequency derived from the NNR. The blocking climatology without the height gradient reversal is also shown in Fig. 3.1b. This is simply calculated by skipping the third step of the sub-section 2). It is evident that overall blocking frequency is substantially, about 25%, overestimated in Fig. 3.1b, indicating that the height gradient reversal effectively reduces the mis-detection of quasi-stationary ridges or immature systems as blocking highs. This is particularly true for PA blockings while a similar change is observed for EA blocking further west (Fig. 3.1c). A similar reduction is also found in high latitude blocking. These results are robust to the choice of threshold value of the gradient reversal (see appendix Fig. A.7). A strong negative threshold value, $Gr(i^*) << 0$, instead of a simple negative reversal yields results that are similar to Fig. 3.1a with only fewer recorded events.

3.4 Results

3.4.1 Blocking climatology

The annual-mean and seasonal-mean blocking frequencies, derived from 50-year long NNR, are presented in Figs. 3.1a and 3.2. They are calculated as the ratio of days a blocked area occupies each grid point to the total number of days per year. Two principal regions of blocking occurrence are evident throughout the year: the one over the northwestern Europe and eastern Atlantic (EA blockings) and the other over the North Pacific (PA blockings). They are located near the end of the Atlantic and Pacific storm tracks. The comparison between the EA and PA blockings further reveals that the EA blockings occur more frequently in a broader region than the PA blockings. In general, blocking occurs more frequently in wintertime than in summertime over both basins (Fig. 3.2).

These results are, at least qualitatively, in good agreement with previous findings (e.g., Dole and Gordon 1983, Tibaldi and Molteni 1990). While this is encouraging as the blocking index employed in this study is somewhat different from the traditional ones, a detailed examination reveals relatively minor but noticeable differences from the previous studies. In comparison to the blocking climatology based on the Dole-Gordon type indices [Croci-Maspoli et al., 2007b, Dole and Gordon, 1983, Sausen et al., 1995], the central region of the EA blockings is extended into western Europe and a weak hint of a third blocking-frequency maximum is present around 50°E in spring and fall, the so-called Ural blocking. Eastern confinement of the EA blockings is somewhat consistent with the blocking climatology derived from the Tibaldi-Molteni type index [Barriopedro et al., 2010b, Pelly and Hoskins, 2003, Tibaldi and Molteni, 1990]. This is due to the effect of the height gradient reversal which reduces the mis-detection of blockings by the Dole-Gordon type index over the western Atlantic (Fig. 3.1c).

The seasonal cycle of the blocking frequency is further examined in Fig. 3.3a. It presents the daily evolution of the NH blocking frequency as a function of longitude. A number of blocking episodes are simply counted along a given longitude band from 30°N to the pole. The resulting time series are then averaged over 50 years and slightly smoothed by applying a running monthly mean filter. Again, two preferred regions of blocking occurrence, the Pacific and the Euro-Atlantic sectors, stand out. The EA blockings are typically more frequent than the PA blockings (see the bottom panel). An exception is summer time when the PA blocking frequency is quite comparable to or even higher than the EA blocking frequency (see also JJA in Fig. 3.2). This peculiar seasonal cycle is consistent with recent studies (e.g., Pelly and Hoskins 2003).

Overall characteristics of individual blocking events are summarized in Fig. 3.4. The duration distribution of events as well as the seasonal cycles of the number of blocking events, mean duration of individual events, and intensity are particularly presented. All statistics are based on blocking onset date: i.e., a blocking episode from January 31st to February 5th is counted as January event. It is found that the number of blocking events decrease almost exponentially as blocking duration increases. As such only few events are found with a time scale of over 10 days (Fig. 3.4a). It is worth noting that the frequency distribution of blockings is also qualitatively similar to that of the negative NAO index [Jia et al., 2007]. In regards to blocking intensity, quantified by the maximum anomaly in an individual blocking lifecycle, winter events are generally stronger than summer events (Fig. 3.4b). This seasonality in part results from our definition of blocking anomalies. In the present study, blocking events are chosen when local anomalies are greater than 1.5 standard deviation at a given month. Since the standard deviation varies with season, with higher values in winter but lower in summer (e.g., dashed contours in Fig. 3.4b), blocking intensity is anticipated to change accordingly.

The average duration and number of blocking events are further shown in Figs. 3.4c and d. A distinct seasonal cycle is found as in previous studies: both number of blocking events and blocking duration exhibit maxima in winter but reach their minima in summer to late summer. Inter-annual variability, as denoted by grey lines, shows significant year-to-year variability with relatively stronger variability in summer. Similar analyses are also performed for the EA and PA blockings separately. It is found that more blocked days over the Euro-Atlantic sector than the north Pacific (Fig. 3.1a and 3.2) is mainly due to more frequent occurrence of blocking there year round (Fig.3.5c). Although EA blockings have a larger number of short lived blocking events (5-9 days, Fig.3.5a), no statistically different mean durations are found year round especially in winter and summer (Fig. 3.5b).

As introduced earlier, long lasting blockings are often associated with extratropical tele-connection patterns. Figure 3.6 illustrates geopotential height anomalies associated with the EA and PA blockings during the cold season. A total of 333 EA and 244 PA blocking events are used to construct the composite map. Statistically significant anomalies, tested with a two-sided students t-test, are observed not only at the blocking regions but also on their equatorward side and far downstream. More specifically EA blockings are accompanied by dipolar geopotential height anomalies over the Atlantic (Fig. 3.6a). This pattern is qualitatively similar to the one associated with the negative phase of the NAO. In contrast, PA blockings are associated with a wave-train pattern over the Pacific and North America. Although this pattern is not exactly same to the PNA, the overall pattern qualitatively resembles the negative phase of the PNA. These results are in good agreement with the previous findings (e.g., Croci-Maspoli et al. 2007b).

3.4.2 GEM model performance

With NNR blocking climatology in hand, this section evaluates the geographical location and seasonal cycle of NH blockings in the GEM model. Only 20 years, from 1987 to 2006, are used as described in the data section. Although 20 years is relatively short, the blocking climatology derived from 20-year data is found to be quantitatively similar to that from 50-year data (compare Fig. 3.7a with Fig. 3.3).

Figure 3.7 shows the longitudinal distribution of blocking occurrence for NNR, GEM model, and their difference. It can be seen that the model captures the overall longitudinal distribution of the blockings and their seasonal variability reasonably well. Nonetheless noticeable differences are present. Most of all, the peak season of blocking activity is delayed from late winter to spring.

This results in an overestimate of blocking frequency over both basins during March and April (Fig. 3.7c). It is also found that, while blocking frequency over the Euro-Atlantic sector is generally *underestimated*, that over the north Pacific it is *overestimated* especially in the cold season. Provided that climate models often underestimate blocking frequency in both basins (e.g., D'Andrea et al. 1998, Scaife et al. 2010), this result is somewhat inconsistent with previous findings. Although Matsueda et al. [2009] showed that the PA blocking frequency can be significantly overestimated in their model, it occurs only when the model is integrated with very high resolution in which high-frequency eddy feedback is likely exaggerated. However, the GEM model, evaluated in this study, has a rather coarse resolution.

To identify the geographical distribution of blocking occurrence in the model, the latitude-longitude distributions of blocking frequency are further illustrated in figure 3.8. Only two seasons, March-April (MA) and October-November-December-January (ONDJ), are presented as the model shows strong biases in these months (Fig. 3.6c). As stated above, PA blocking frequency is significantly overestimated both in MA and ONDJ. This sharply contrasts with the EA blocking whose frequency is generally underestimated by the model with an enhancement over southern Europe. The result of these biases is that, during the cold season, the maximum frequency of PA blockings is somewhat larger than that of the EA blockings in the model. It is also found from Fig. 3.8 that preferable regions of blocking activity are slightly shifted equatorward in both basins. An eastward extension is also evident over the north Pacific. These results suggest that the model biases illustrated in Fig. 3.7c are caused not only by inaccurate representations of blocking frequency but also by misrepresentations of blocking regions by the model. These biases further cause the biases in the teleconnection pattern in association with blocking highs. The PNA-like pattern associated with PA blockings exhibits stronger amplitude than the NNR with slight eastward extension (compare Fig. 3.6b with Fig. 3.9b). Likewise, the NAO-like pattern over the Euro-Atlantic sector is weaker and shifted slightly eastward in the model (compare Fig. 3.6a with Fig. 3.9a).

Figure 3.10 presents the number of blocking events in the NH as a function of duration. The lifetime distribution of the modelled blockings exhibits an exponential decrease with blocking persistence (see also Fig. 3.4a). This is in good agreement with the NNR. While small differences are found for blocking events with a timescale of 6 to 9 days, it is statistically insignificant. Decomposition of the lifetime distribution by basin reveals these differences resulting from a slightly larger number of PA blocking events (Fig. 3.11d). Figure 3.11 further shows the seasonal cycles of individual blocking duration and number of events for the GEM model in good agreement with the NNR (Fig. 3.11b,c,e,f). The results suggest that the GEM model reproduces overall characteristics of individual blocking events reasonably well if they occur.

3.5 Possible sources of error

Ascribing model biases to physical causes is difficult to achieve without systematic model experiments by varying model resolution, physical parametrization and boundary conditions. Regardless of model configuration, however, there are general sources of error that lead to biases in low-frequency variability. For blocking highs, it is well known that misrepresentation of the time-mean flow and high-frequency eddies could be culprits of model biases in blocking frequency, intensity and duration (e.g., Barriopedro et al. 2010b). As such, this section attempts to relate the model biases in blocking climatology with those in time-mean flow and transient eddies. In order to better understand overestimate of PA blocking, the energetics are also briefly discussed.

3.5.1 Time-mean flow and transient eddies

Figure 3.12 presents stationary eddies at 500 hPa, defined by the zonally asymmetric component of the climatological geopotential height field, during ONDJ (top) and MA (bottom row) for NNR (left), GEM model (middle) and their difference (right column). It is found that stationary eddies, with primarily components of zonal wave number one (k=1) and two (k=2), are reasonably well reproduced by the model. Noticeable differences are however observed over the eastern North Pacific and Euro-Atlantic regions (Figs. 3.12c,f). The model biases, which do not exactly mirror blocking biases shown in Figs. 3.8c,f, are dominated by k=1 in relatively low latitudes. In high latitudes, they exhibit k=2 pattern.

A key feature of modelled stationary eddies in ONDJ is its eastward shift in comparison to NNR (Figs. 3.12a-c), concurrent with the overall shift in blocking activity centers to the east (Figs. 3.8a-c). Strong negative biases are particularly evident over the central North Pacific and Northern Europe as a result of a deeper Pacific trough and a split in the Euro-Atlantic ridge. By referring to NNR, these biases project positively onto the Pacific trough but negatively onto the Euro-Atlantic ridge, although they are slightly shifted to the east. This opposite projection is more clearly illustrated in Fig. 3.13 where stationary eddies are integrated from 30°N to 70°N to isolate their longitudinal structure. Decomposition of stationary eddies into k=1 and k=2 components indicates that the model biases in ONDJ are dominated by k=2 component with an additional contribution by k=1 component from mid-October to mid-November. The opposite projection of model biases to climatological background flow over the two basins has important implications to model blocking biases. For instance, if blocking highs are the result of the resonant interaction between quasi-stationary and transient eddies [Austin, 1980, Cash and Lee, 2000], this would provide a preferable condition for more frequent blocking over the Pacific (through stronger interaction) but less frequent blocking over the Euro-Atlantic regions in accordance with model blocking biases during ONDJ (Fig. 3.8c). Note that this consistency does not provide a causal relationship as biases in stationary eddies are partly caused by blocking biases themselves.

During MA, the model exhibits a significant eastward and equatorward shift in stationary eddies (Figs. 3.12d-f) as in blocking bias (Figs. 3.8d-f). This misplacement is primarily due to k=1 component (Fig. 3.13c). Contribution by other wave numbers is essentially absent. It is also found that model biases largely result in a deeper than normal trough over the Pacific and higher than normal ridge over the Euro-Atlantic regions. In other words, in contrast to ONDJ bias, model bias in these months projects positively over the two basins. It supports a resonance argument: resonance interaction between quasi-stationary and transient eddies may be enhanced in the model during MA. This is again consistent with more frequent blocking activities over the two basins.

The mean-flow bias is further examined in Fig. 3.14 with regards to the climatological jets at 500 hPa. Although the model is able to reproduce westerly jets reasonably well, both the Pacific and Atlantic jets are somewhat overestimated at the exit regions. This is simply due to the southeastward extension of the Pacific jet in the model in both ONDJ and MA and to the eastward extension of the Atlantic jet in ONDJ. Not surprisingly, this is consistent with the geopotential height field as shown in Fig. 3.12. An equatorward shift of the Pacific jet in both seasons (Figs. 3.14b,e) may have an important implication for blocking climatology there. Specifically this may provide a preferable condition for more frequent blocking consistent with model blocking biases. Kaas and Branstator [1993] indicated that a background flow with an equatorward-shifted jet tends to allow more frequent blocking occurrence. An eastward extension of the Atlantic jet, especially in ONDJ (Fig. 3.14b), would play an opposite role. The zonally-elongated and strengthened jet weakens diffluence at the exit region of the jet, preventing blocking formation there (compare stream function in Figs. 3.14a and 3.14b).

Next we examine the model biases in transient eddies (Fig. 3.15). Transient eddy activities are quantified in this study by using the variance of 500-hPa geopotential height anomalies. High-frequency (period shorter than 10 days) and low-frequency eddies (10-90 days) are examined separately to highlight their difference. It can be seen that the longitudinal distribution of low-frequency eddy activity is quite similar to that of blocking frequency (compare Figs. 3.7 and 3.15a-c). Its biases also resemble blocking biases reasonably well. For instance, Atlantic-Pacific blocking biases in ONDJ and seasonal delay in MA are evident in low-frequency eddies. It is noteworthy that, unlike the blocking frequency climatology, low-frequency eddy activity is somewhat stronger over the Pacific than over the Atlantic during January-February. This difference is not surprising as not all low-frequency eddy activities are associated with blocking highs. In addition, the low-frequency eddy activities include information about amplitude whereas the blocking frequencies include only frequency information (although individual blockings have to satisfy an amplitude criterion). This may be an additional reason why there is a difference between low-frequency eddy activities and blocking frequencies.

The model successfully reproduces the seasonal cycle of both Atlantic and Pacific storm tracks (Figs. 3.15d-f). However it underestimates high-frequency eddies in all seasons and almost everywhere. This underestimate is particularly strong over the Euro-Atlantic region during ONDJ. If blocking highs are forced and maintained by high-frequency eddies (e.g., Nakamura et al. 1997), this result would provide an additional explanation for why EA blocking frequency in ONDJ is substantially underestimated. Although it does not explain the overestimation of PA blocking in ONDJ and the seasonal delay of EA and PA blockings in MA. This indicates that the role of high-frequency eddies on blocking formation and maintenance may differ with seasons and geographical locations.

3.5.2 Energetics

The above result suggests that the overestimation of PA blocking is more likely associated with biases in time-mean flow rather than high-frequency eddies. To better understand the possible impact of time-mean flow bias on PA blocking frequency, this section briefly examines energetics at 500 hPa.

A number of studies have shown that two major sources of low-frequency eddy kinetic energy (EKE) at the exit regions of westerly jets, where blocking frequency forms most frequently, are barotropical energy conversion (BTC) from the time-mean flow and non-linear energy transfer from high-frequency eddies to low-frequency eddies [Sheng and Derome, 1991a,b, Simmons et al., 1983]. For BTC, Simmons et al. [1983] have particularly shown that the longitudinally-varying background flow plays a crucial role. Since blocking highs can be qualitatively understood by low-frequency eddy activities (Figs. 3.15a-c), blocking biases are related to time-mean flow biases by analyzing BTC below.

The barotropic energy conversion from the time-mean flow to transient eddies, is given by:

$$BTC = -(\overline{u'^2} - \overline{v'^2}) \left[\frac{1}{a\cos\phi} \frac{\partial \bar{u}}{\partial \lambda} - \bar{v} \frac{\tan\phi}{a} \right] - (\overline{u'v'}) \left[\frac{\cos\phi}{a} \frac{\partial}{\partial \phi} \left(\frac{\bar{u}}{\cos\phi} \right) + \frac{1}{\cos\phi} \frac{\partial \bar{v}}{\partial \lambda} \right] \tag{3.4}$$

where u and v are the zonal and meridional wind components respectively, overbars represent a time average, primes denote deviations from the time mean, λ is the longitude, ϕ is the latitude and a is the radius of the earth [Simmons et al., 1983]. It is shown by Simmons et al. [1983] that equation (1) can be simplified in the mid-latitudes to a good approximation to the form:

$$BTC \simeq \mathbf{E} \cdot \nabla \bar{u} = -(\overline{u'^2} - \overline{v'^2}) \frac{1}{a\cos\phi} \frac{\partial \bar{u}}{\partial \lambda} - (\overline{u'v'}) \frac{1}{a} \frac{\partial \bar{u}}{\partial \phi} \tag{3.5}$$

where $\mathbf{E}$ denotes the E-vector in Hoskins et al. [1983]. The first term on the right hand side describes energy transfer due to anisotropy of the disturbances and zonally-varying background flow. Transient eddies extract KE from the mean flow when zonally elongated eddies ($\overline{u'^2} > \overline{v'^2}$) occur in the region of diffluence ($\partial\bar{u}/\partial\lambda < 0$). This contrasts with the second term on the right hand side that is the classical BTC from the zonally uniform flow to the eddies by an upgradient eddy momentum flux.

Figure 3.16 presents low-frequency **E**-vectors superimposed on climatological zonal wind during ONDJ and MA. Significant low-frequency eddy activities are observed at the exit regions of the westerly jets. In ONDJ, the model shows stronger westerlies over the central North Pacific and western Europe than NNR (Fig. 3.16c; see also Fig. 3.14c). This excessive zonal wind results in enhanced stretching deformation over the eastern North Pacific and reduced deformation over the central North Atlantic. Since **E**-vectors in these regions are directed westward, this background flow allows more effective BTC over the eastern North Pacific but less effective BTC over the eastern North Atlantic. Enhanced westward **E**-vectors in the viscinity of west coast of North America where westerlies decrease with longitude ($\partial\bar{u}/\partial\lambda < 0$) and near Iceland where westerlies slightly increase with longitude ($\partial\bar{u}/\partial\lambda > 0$) also likely contributed to dipolar biases in blocking frequency over the two basins. This is consistent with blocking biases during ONDJ (Fig. 3.8c). A similar argument also holds for PA blocking during MA (Fig. 3.16d-f), although EA blocking cannot be simply explained by BTC.

3.6 Summary and conclusions

The performance of the Global Environmental Multiscale (GEM) model is evaluated in this study in the context of the Northern Hemisphere (NH) blocking climatology. Geographical distribution, seasonal cycle and statistics of individual blocking events are quantitatively compared with those derived from the NCEP-NCAR Reanalysis (NNR). This comparison is conducted by applying a newly developed blocking index to the GEM and NNR data in a same resolution.

The blocking index developed in this study is a kind of hybrid index which combines the two widely-used blocking indices, namely the Dole-Gordon and Tibaldi-Molteni indices, in a simple way. Specifically blocking highs are identified by assuring the latitudinal gradient reversal in 500-hPa geopotential height field, as in the Tibaldi-Molteni type index, on the equatorward side of blocking anomalies which are defined by the Dole-Gordon type index. This approach effectively removes quasi-stationary ridges which are often misdetected as blockings in the Dole-Gordon type index. It also allows us to detect omega-shape blockings which are often ignored in the Tibaldi-Molteni type index.

It is found that the GEM model is able to reproduce individual blocking events reasonably well. The total number of NH blocking events and their duration and intensity are quantitatively well simulated in comparison to the NNR. However, significant biases are found in blocking frequency over the two basins with seasons. The biases can be summarized in three key aspects: (1) The peak season of blocking activity is delayed from winter to early spring in both basins. (2) The Euro-Atlantic (EA) blocking frequency is generally underestimated in the cold season. (3) The north Pacific (PA) blocking frequency is overestimated in most seasons. The last point, the overestimate of the PA blockings, is the most peculiar finding in this study as numerical models typically underestimate blocking activity over both the Euro-Atlantic and north Pacific basins [Barriopedro et al., 2010a, D'Andrea et al., 1998, Doblas-Reyes et al., 2002, Scaife et al., 2010]. Although Matsueda et al. [2009] showed an example of overestimated PA blocking frequency in their model, it was found only in a very high-resolution model integration, much higher than the one used in the GEM model.

The model blocking biases are found to be largely associated with the biases in the time mean flow. More specifically stationary wave activity in the model exhibits a seasonal delay and equatorward shift in zonal wavenumber one component. This is consistent with the seasonal delay in maximum blocking frequency in both basins. In high latitudes, zonal wavenumber two component shows an eastward shift, yielding a deeper than normal trough over the north Pacific and shallower than normal trough over the north Atlantic. This likely results in a stronger interaction between quasi-stationary waves and transient waves over the north Pacific but a weaker interaction over the north Atlantic, possibly explaining anomalous blocking activity over the two basins with opposite sign during most seasons. Although this does not provide a causal relationship as the mean-flow biases may simply result from the blocking biases themselves, a similar consistency is not found in high-frequency eddies which are underestimated over both basins in most seasons. This indicates that the possible non-linear energy transfer from high-frequency transient eddies to quasi-stationary blocking anomalies may not be a direct cause of the overestimate of PA blocking in ONDJ and the seasonal delay in PA and EA blocking in late winter, although it may play a role in cold season EA blocking which is underestimated by the model.

The importance of the time-mean flow in blocking biases is further supported by the energetics. It is particularly found that the model biases in PA blocking frequency are consistent with barotropic energy conversion from the mean flow to low-frequency eddies. The model shows an southeastward extension of the Pacific jet in most seasons. Westerly biases are also evident over Europe in the cold season. These biases result in stronger (weaker) stretching deformation over the north Pacific (eastern Atlantic-Europe), causing stronger (weaker) barotropic energy transfer from the time-mean flow to the low-frequency eddies there. However a corresponding energy transfer for the EA sector in March and April is not clear.

The causes of time-mean flow and transient eddy biases, which are inherently linked to blocking biases as summarized above, are not addressed in this study. They could result from insufficient model resolution, unrealistic physics, prescribed (not interactive) surface boundary conditions, etc. To address these issues, systematic model sensitivity tests would be needed. This is however beyond the scope of the present study.

It should be stated that overall results reported here could be sensitive to the choice of blocking index. In fact, north Pacific blocking biases become much smaller when a classical Tibaldi-Molteni index is applied. This likely results from the ignorance of omega shaped blocking in the Tibaldi-Molteni index. Likewise, if a blocking index is applied to a dynamic variable in the upper troposphere (e.g., potential vorticity on the 2 PVU surface), instead of a thermodynamic variable in the mid-troposphere as done in this study, quantitatively different results could emerge. However, given the similarity between the blocking climatology found in this study and low-frequency variability at 500 hPa (Figs. 3.7c and 3.15c), we believe that overall results would not change substantively.

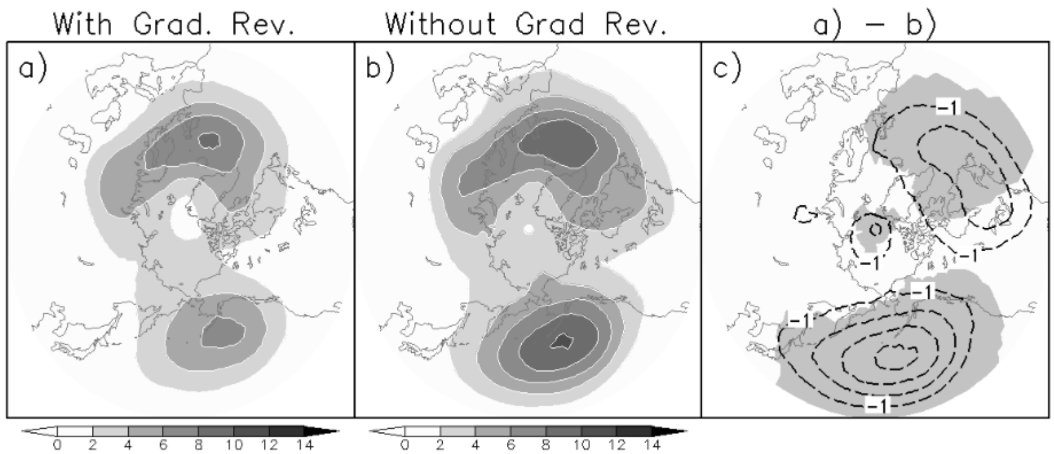

Figure 3.1: Climatology of NH annual-mean blocking frequency for NNR over the period of 1960-2010: a) blocking index with height gradient reversal, b) blocking index without height gradient reversal and c) their difference. Shading interval in a) and b) is in percent of days per year. Bias contour interval in c) is 1 percent of days per year. Shaded areas in c) denote statistically significant differences at the 95 percent confidence level using a two-tailed student t-test.

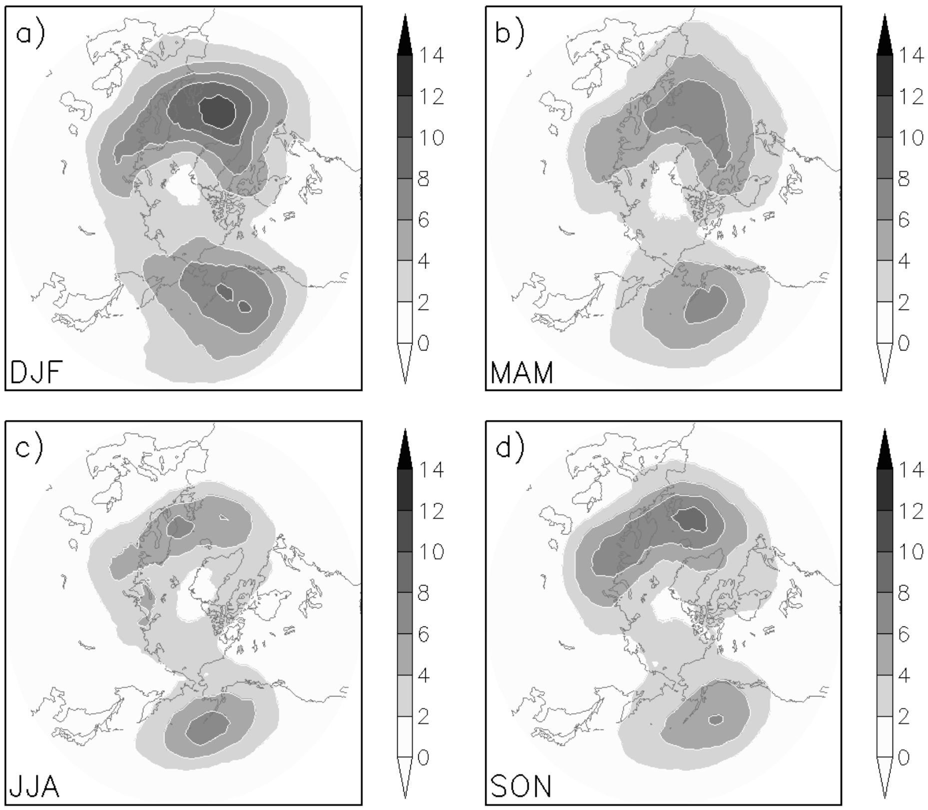

Figure 3.2: Climatology of seasonal-mean NH blocking frequency from NNR: a) DJF, b) MAM, c) JJA and d) SON. Shading interval is in percent of days per season.

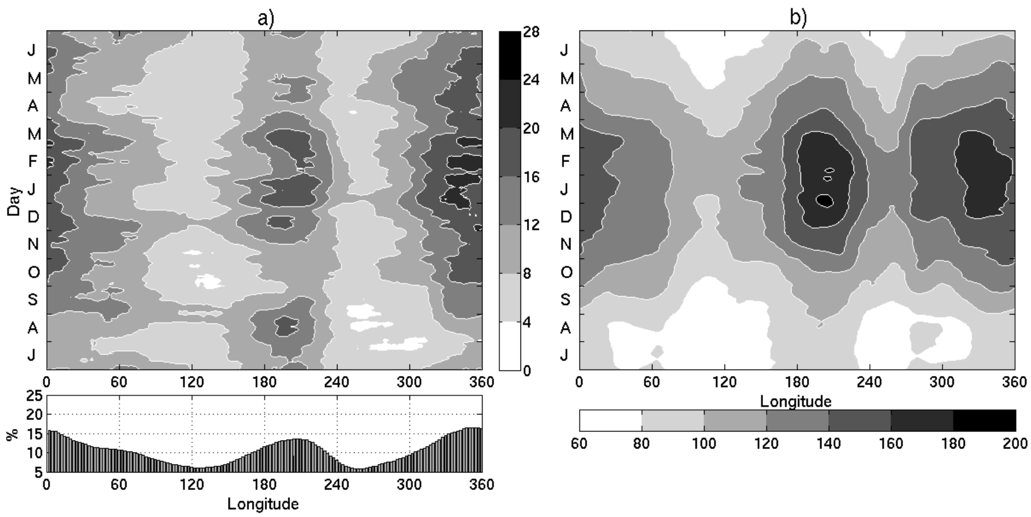

Figure 3.3: (a) (top) seasonal cycle and (botttom) annual-mean of the NH blocking frequency as a function of longitude from NNR. Shading interval is in percent of days per 30 days centered on a given day. (b) seasonal cycle of NH low-frequency eddies from NNR.

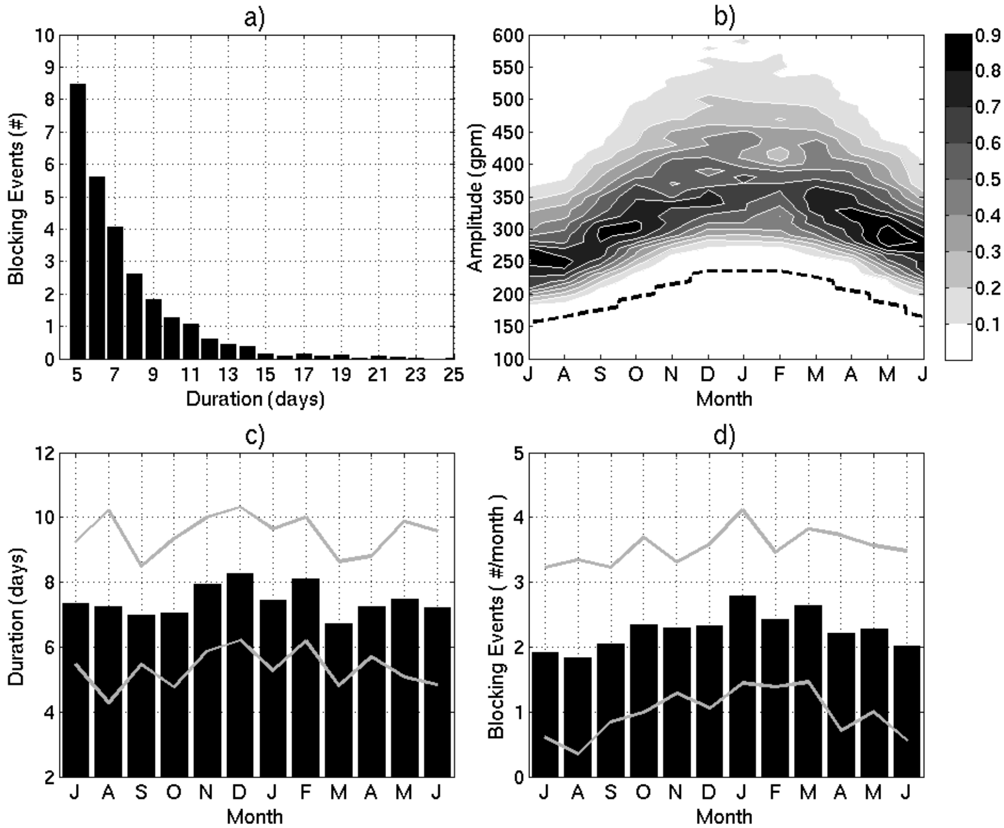

Figure 3.4: Overall characteristics of individual NH blocking events from NNR: a) annual number of events by duration, b) number of events by intensity and month, c) duration of events by month and d) number of events by month. Dashed contours in b) represent monthly anomaly thresholds used in the blocking index. In (c,d), interannual variability, measured by one standard deviation, is shown with grey lines.

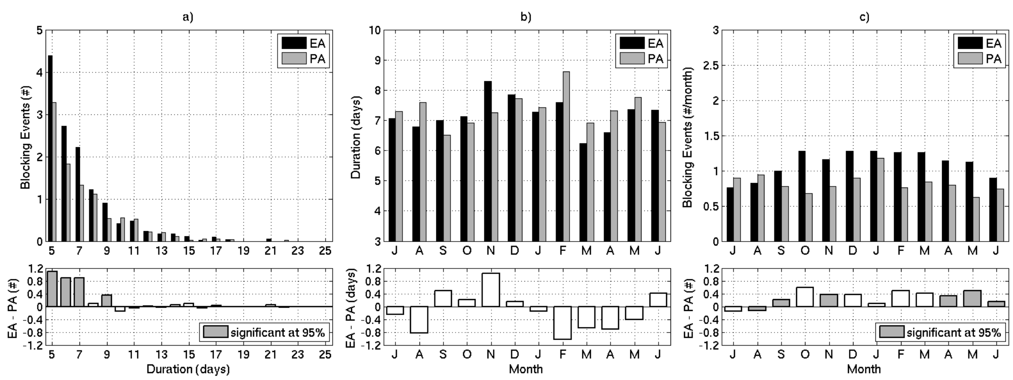

Figure 3.5: (Top) Overall characteristics of individual NH blocking events from NNR for the EA (black) and PA (grey bars) sectors and (bottom) their difference : a) annual number of events by duration, b) duration of events by month and c) number of events by month. Shaded grey bars in the bottom figures denote values that are statistically significant at the 95 percent confidence level using a two-tailed students t-test.

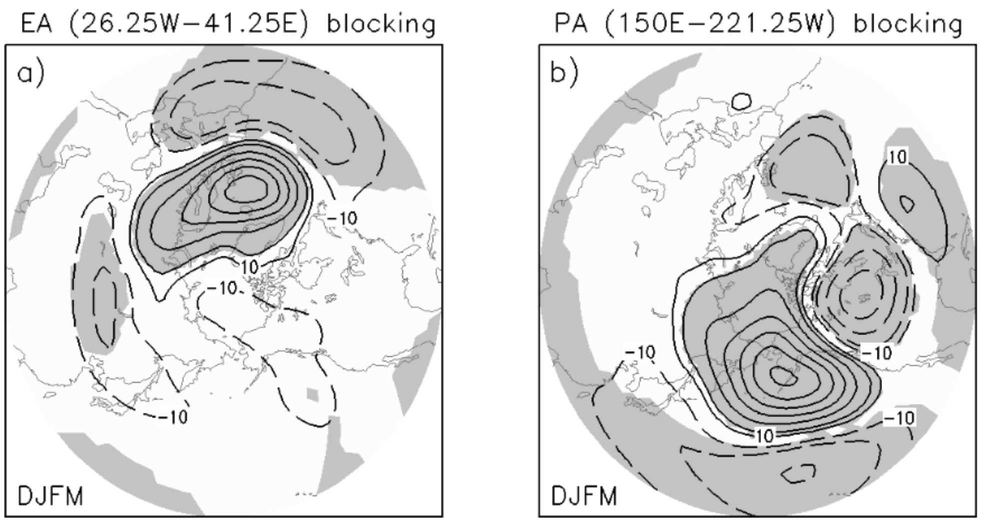

Figure 3.6: DJFM 500-hPa geopotential height anomalies associated with a) EA blocking and b) PA blocking events for 50-year long NNR. Contour interval is 10 m and the zero lines are omitted. Shading denotes anomalies which are significantly different from zero at the 95 percent confidence level using a two-tailed student t-test.

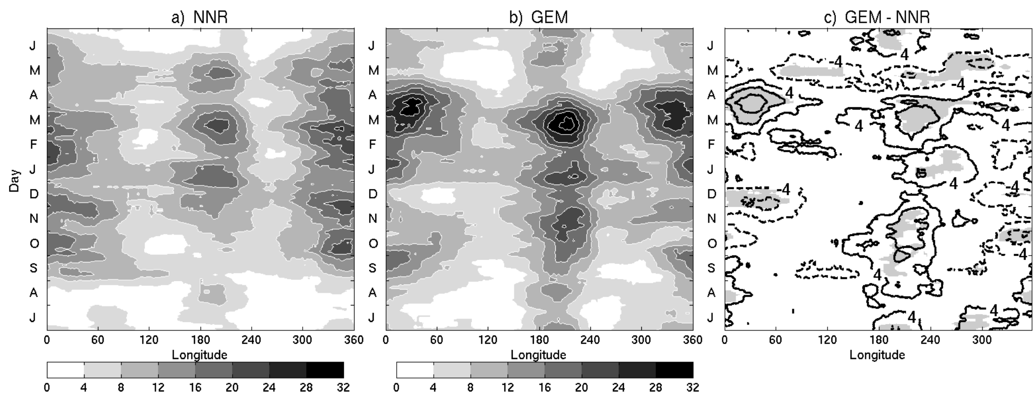

Figure 3.7: Seasonal cycles of NH blocking frequency for the period of 1987-2006: a) NNR, b) model and c) their difference. Shading interval is 4 percent of days per 30 days centered on a given day. Contour interval in c) is 4 percent and the zero lines are ommited. values that are statistically significant at the 95 percent confidence level are shaded.

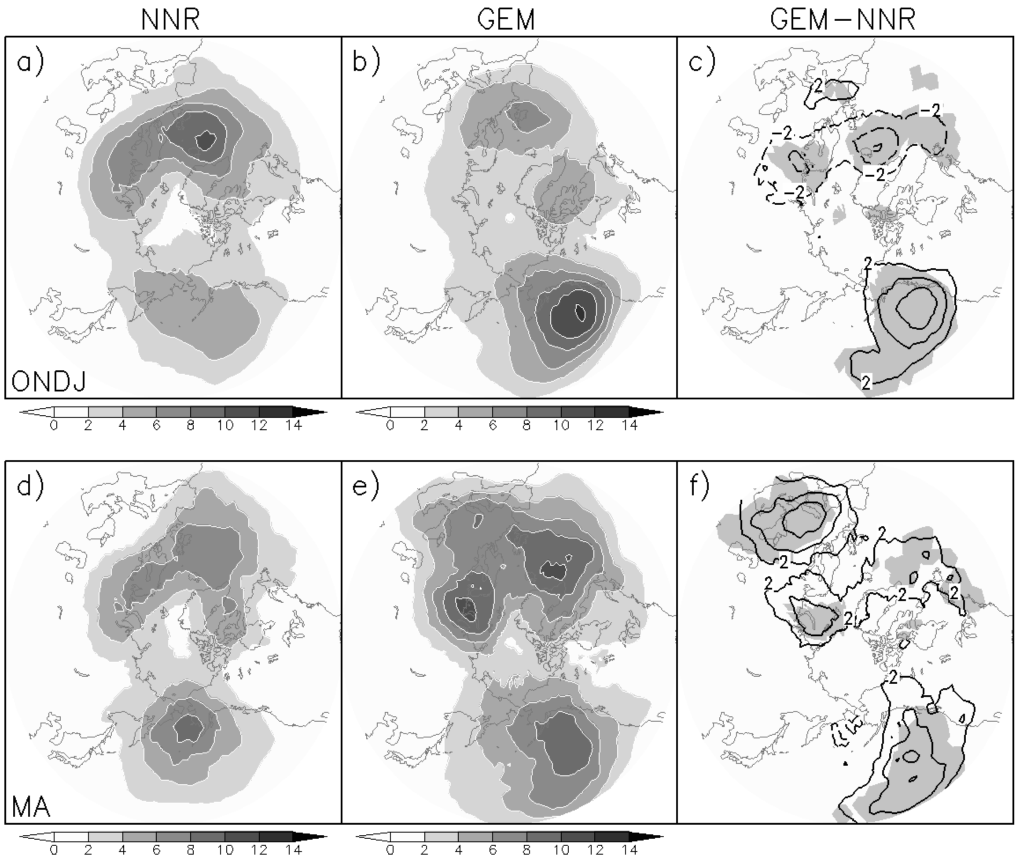

Figure 3.8: Climatology of NH blocking frequency: (a,d) NNR, (b,e) GEM model and (c,f) their difference during (a-c) ONDJ and (d-f) MA. Shading is in units of percent of days per season. Contour interval in (c,f) is 2 percent and the zero lines are omitted. values that are statistically significant at the 95 percent confidence level using a two-tailed t-test are shaded.

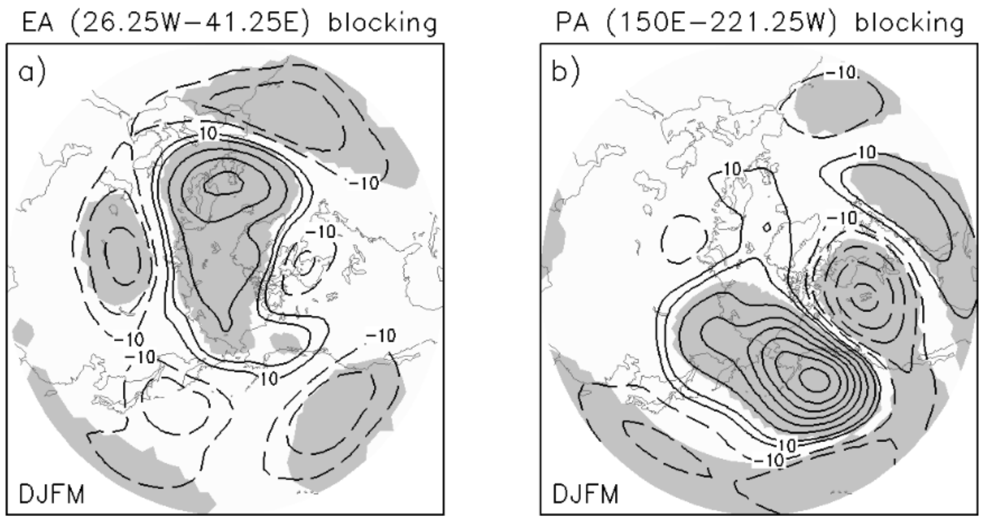

Figure 3.9: DJFM 500-hPa geopotential height anomalies associated with a) EA blocking and b) PA blocking events for 20-year long GEM data. Contour interval is 10 m and the zero lines are omitted. Shading denotes anomalies which are significantly different from zero at the 95 percent confidence level using a two-tailed student t-test.

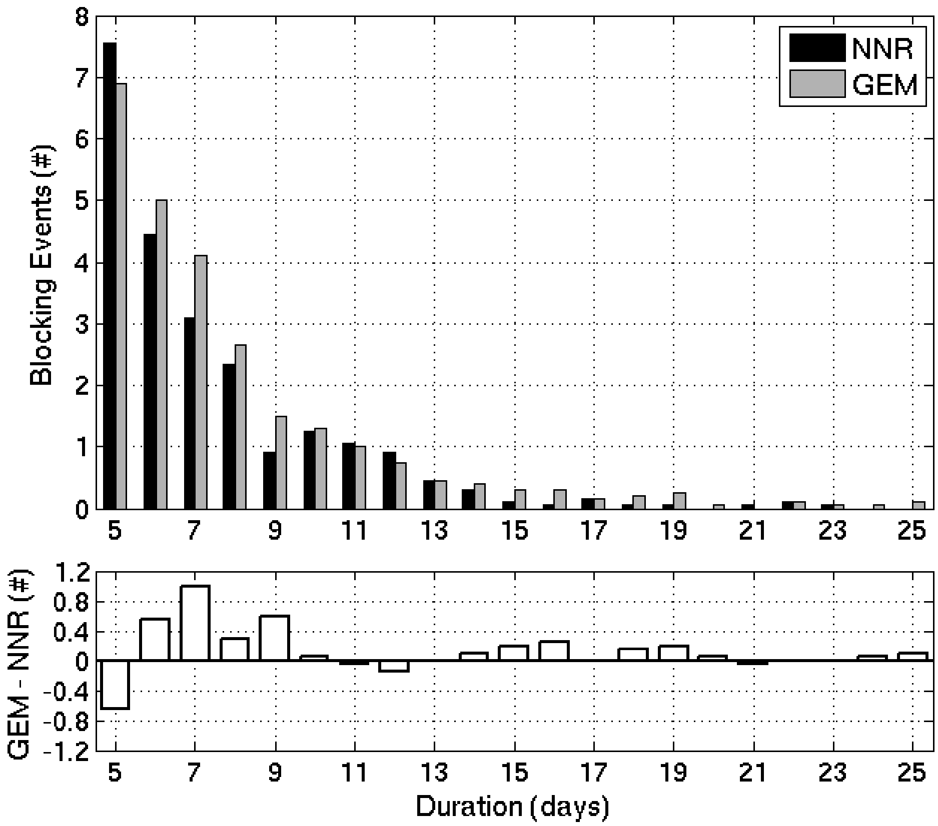

Figure 3.10: Number of blocking events as a function of duration for NNR (black) and model (grey bars), and their difference.

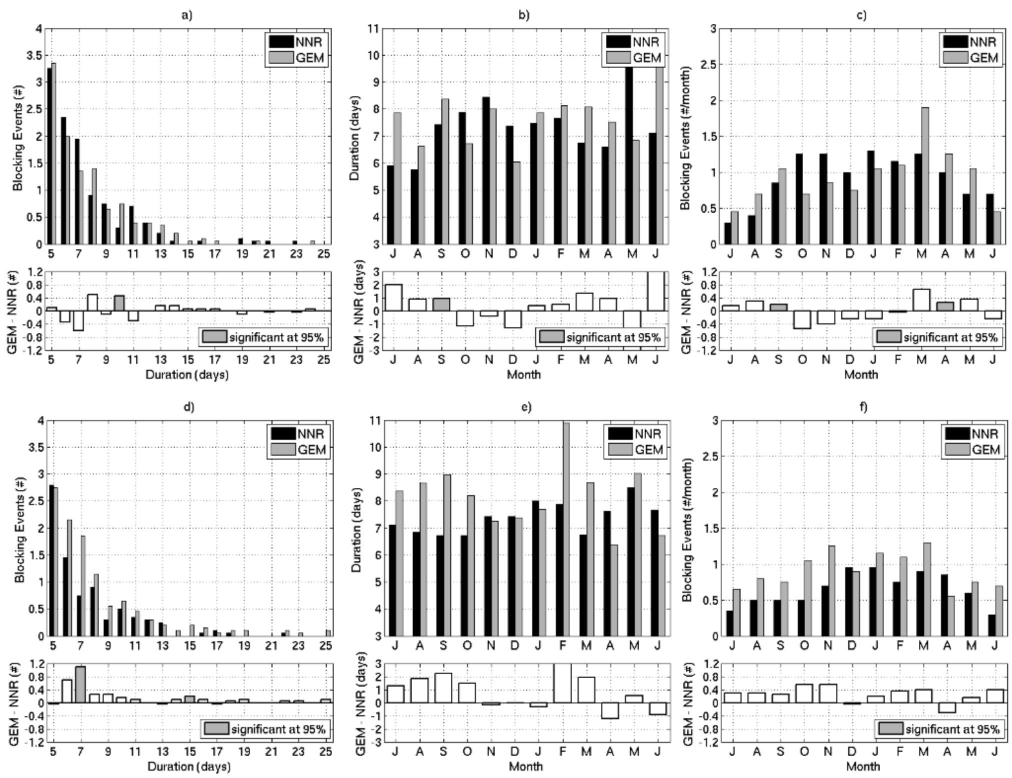

Figure 3.11: (a-c) EA and (d-e) PA sector characteristics of individual NH blocking events from NNR (black) and GEM model (grey bars) and their difference: (a,d) annual number of events by duration, (b,e) duration of events by month and (c,f) number of events by month. Shaded grey bars in the bottom of figures denote values that are statistically significant at the 95 percent confidence level using a two-tailed students t-test.

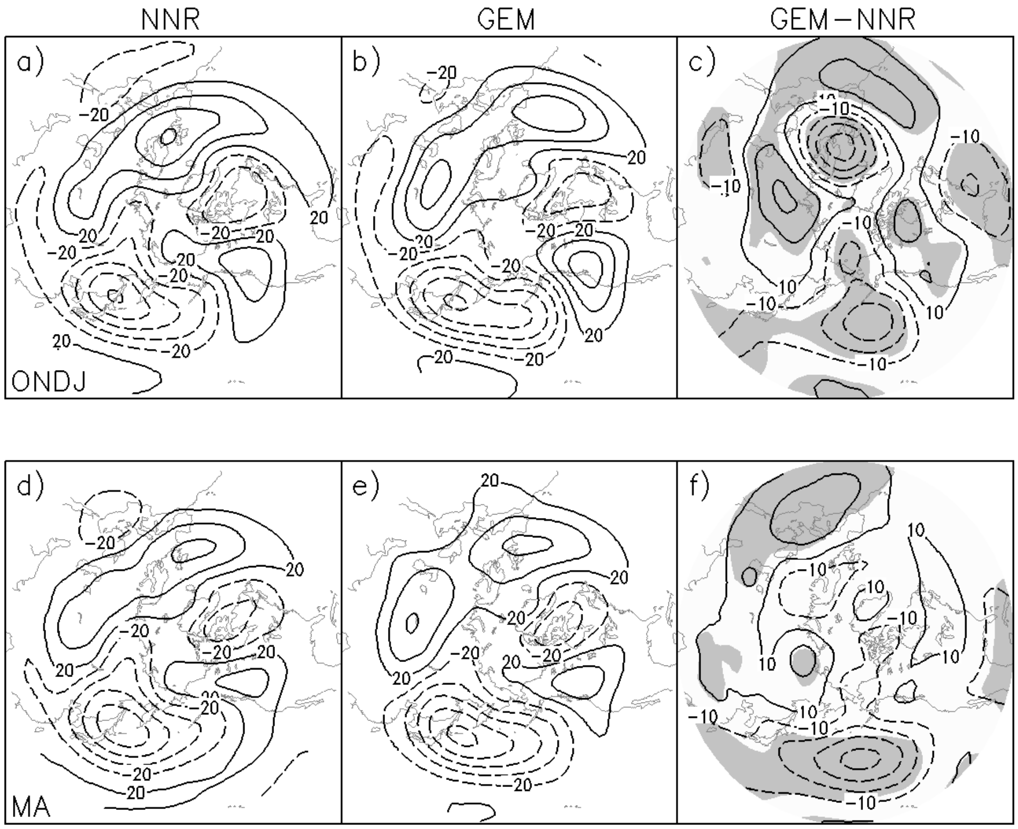

Figure 3.12: Stationary eddies for (a,d) NNR, (b,e) GEM model and (c,f) their difference during (a-c) ONDJ and (d-f) MA. Contour interval in (a,b,d,e) is 20 m. Contour in (c,f) is 10 m and values that are statistically significant at the 95 percent confidence level are shaded. Zero lines are omitted in all figures.

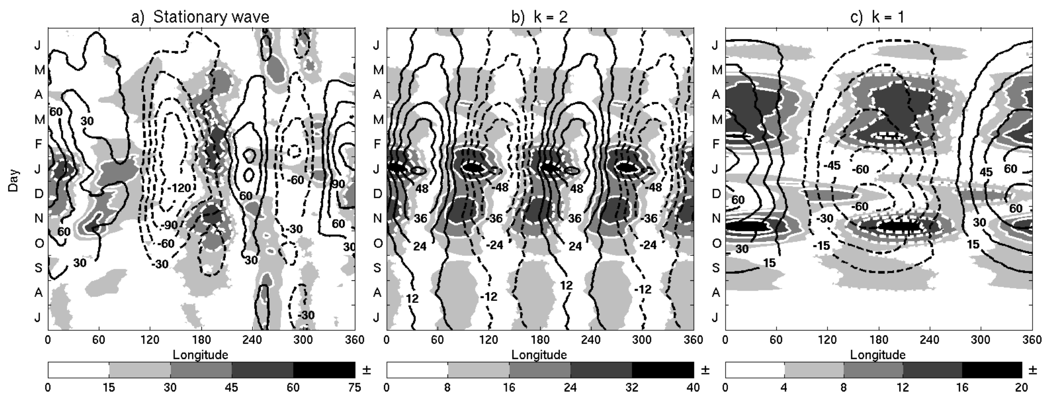

Figure 3.13: Seasonal cycles of stationary eddies integrated from 30°-70°N: a) full, b) k=2 and c) k=1 components. NNR climatology is contoured and model biases (GEM-NNR) are shaded in grey. Positive and negative biases are denoted with solid and dashed white contours, respectively. Zero lines are ommitted in all figures.

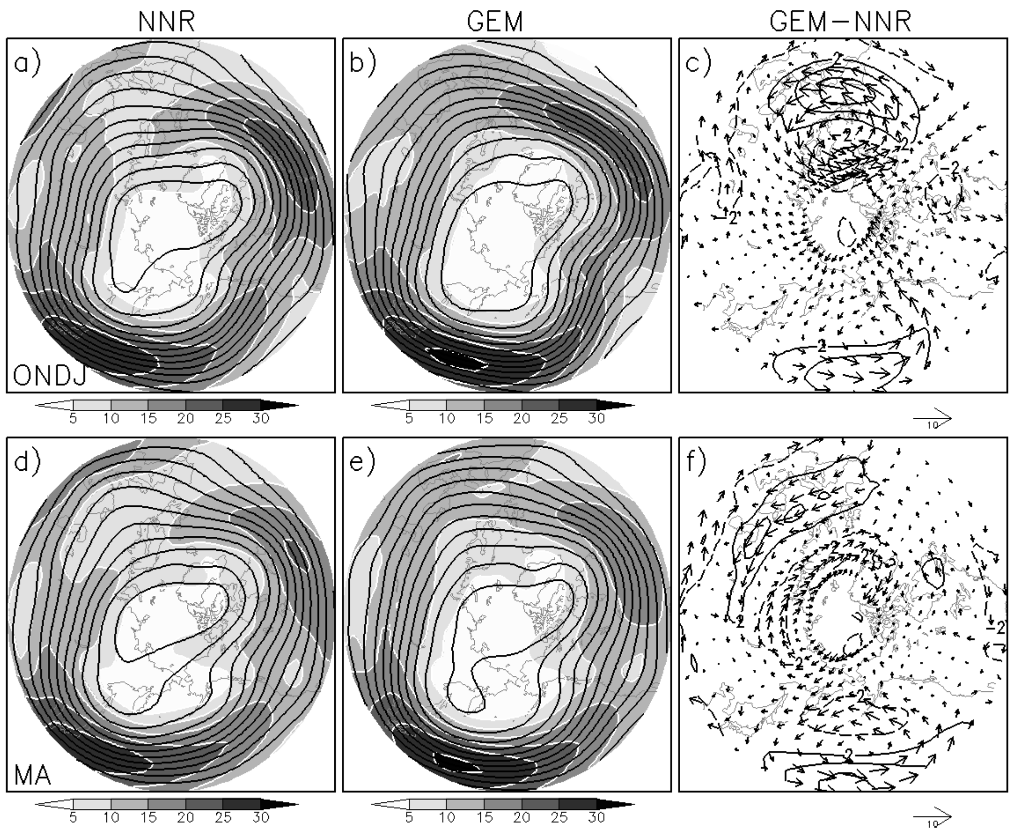

Figure 3.14: Climatology of NH zonal wind (shading), streamfunction (contours) and wind vector at 500 hPa for (a,d) NNR, (b,e) GEM model and (c,f) their difference during (a-c) ONDJ and (d-f) MA. Stream function contour interval is 10^6 m$^2 s^{-1}$ in (a,b,d,e). Zonal wind contour interval in (c,f) is 2 ms^{-1}.

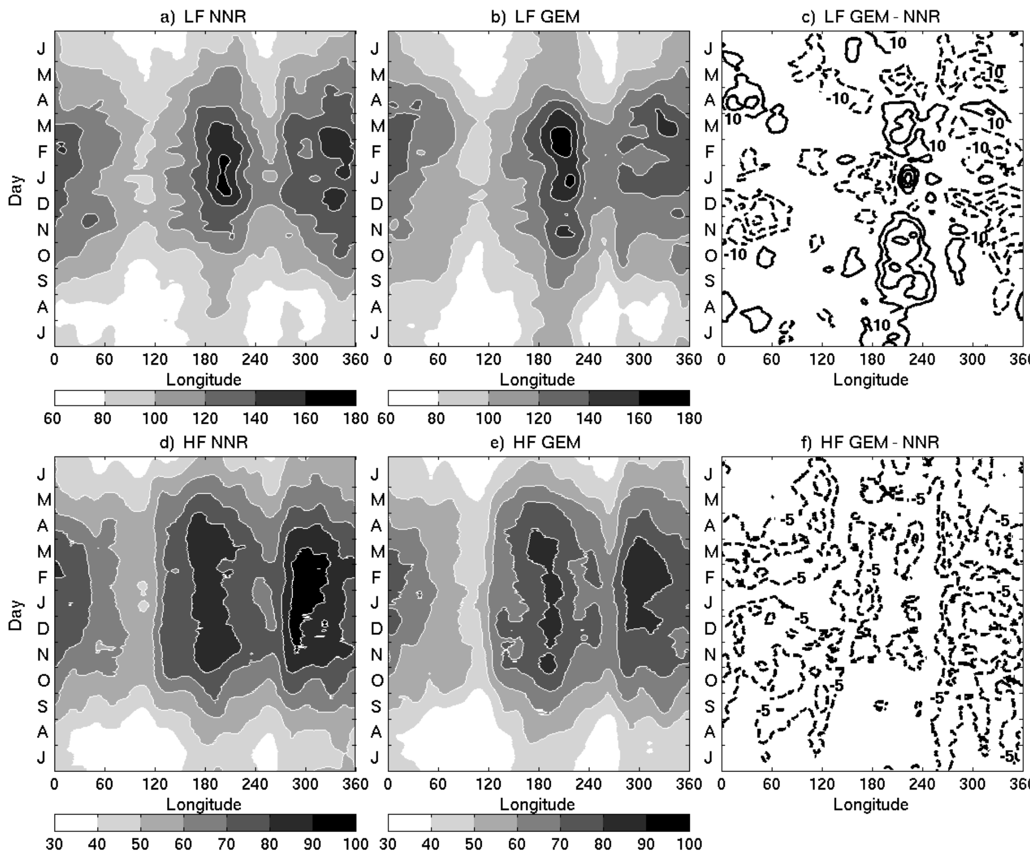

Figure 3.15: Seasonal cycles of (a-c) low-frequency (LF) and (d-f) high-frequency (HF) eddies for (a,d) NNR, (b,e) GEM model and (c,f) their difference. Contour intervals in (c,f) are 10 m and 5 m respectively. Zero lines are ommitted.

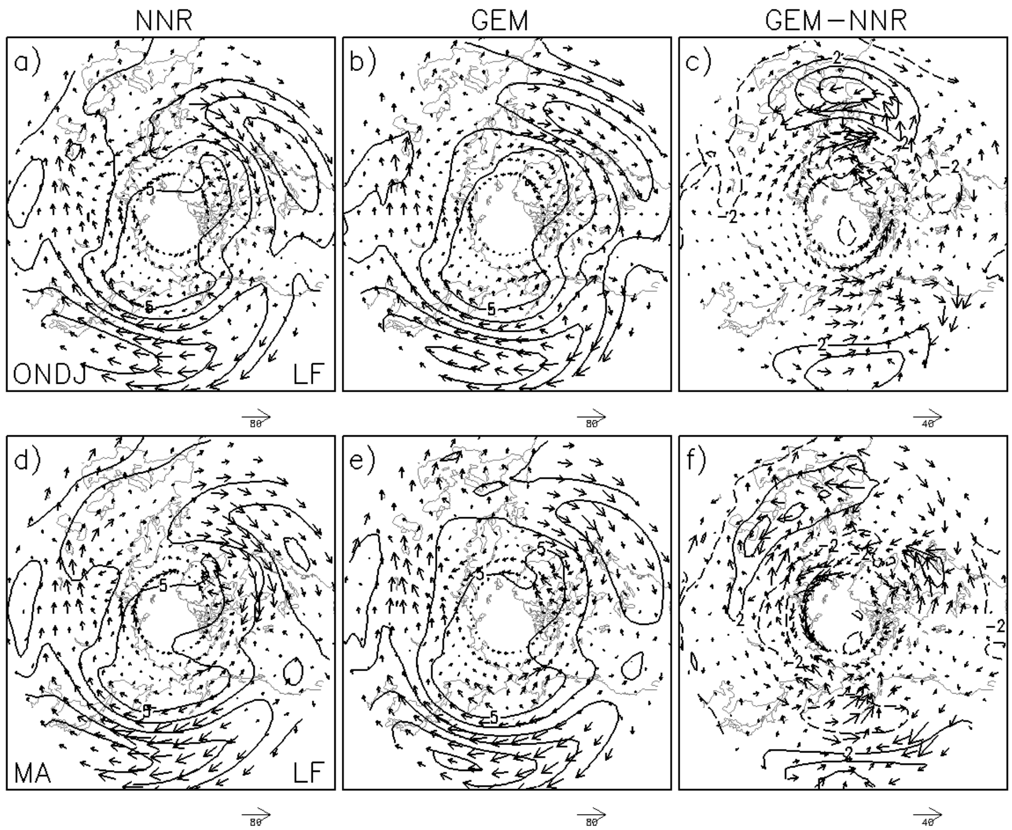

Figure 3.16: Climatological zonal wind (contours) and low-frequency E-vectors for (a,d) NNR, (b,e) GEM model and (c,f) their difference during (a-c) ONDJ and (d-f) MA. Contour interval in (a,b,d,e) is 5 ms^{-1}. Contour interval in (c,f) is 2 ms^{-1}. Zero lines are ommitted.

Chapter 4

Northern Hemisphere blocking climatology in the present and future climate as simulated by the CMIP5 models

From the results in chapter 3, we now have confidence in the capacity of our blocking index to reliably identify blocking events in long-term climatological data sets. As such, we extend our analysis of Northern Hemisphere blocking climatology to the current and future simulations of the latest generation of climate models participating in the coupled model inter-comparison project phase 5 (CMIP5).

Abstract

Preliminary analyses of Northern Hemisphere blocking climatology are undertaken using a subset of climate models participating in the Coupled Model Inter-comparison Project phase 5 (CMIP5). Both historical and RCP8.5 runs are examined to evaluate the performance of the CMIP5 models in comparison to NNR and to identify possible changes in blocking frequency and duration in a warm climate. This is achieved by applying a comprehensive but still relatively simple blocking index to both model historical and RCP8.5 integrations. Comparison to reanalysis reveals that most models can reproduce the Northern Hemisphere blocking climatology reasonably well although maximum Euro-Atlantic blocking frequency is generally underestimated during the cold season. Significant overestimation of maximum Pacific blocking frequency is also evident throughout the year in some models. In contrast, RCP8.5 integrations show a weak hint of reduced blocking frequency over the Pacific sector as compared to historical integrations. However, no clear seasonality in Pacific sector blocking frequency change is observed. Additionally, no significant difference is found in terms of block duration within the RCP8.5 integrations.

4.1 Introduction

Atmospheric blockings, characterized as persistent quasi-stationary synoptic scale high pressure systems, are a marked feature of extratropical low frequency variability. Lasting days to weeks, a blocking high remains quasi-stationary relative to the background flow, interrupting the eastward progression of synoptic scale systems causing them to divert meridionally there. These persistent high pressure systems largely occur at the ends of the climatological storm tracks over the northeastern Atlantic and Pacific basins, often inducing a split westerly jet.

The impact of atmospheric blocking on surface weather and extratropical circulation is well documented (e.g., Rex 1950b, Stein 2000, Trigo et al. 2004). Blocking highs are associated with significant temperature anomalies beneath the block as well as increased precipitation and storm activity around the block. Exceptionally long-lasting blocking events can also engender significant changes in surface conditions, relevant to human society. Striking examples include the recent 2003 European and 2010 Russian heat waves resulting from persistent blocking episodes, both of which lead to record breaking temperatures and large increases in mortality rates in the surrounding area [Black et al., 2004, Dole et al., 2011]. The latter case further contributed to largescale crop damage [Matsueda, 2011] and has also been suggested as a culprit of catastrophic flooding in Pakistan, due to its concomitant downstream trough [Webster et al., 2011].

The above-described importance of blocking underlines the need for the reliable simulation of blocking highs in climate studies. It is well known that there are systematic biases in blocking frequency in the previous generation of GCM's [D'Andrea et al., 1998, Scaife et al., 2010] and it has been found that the misrepresentation of the time-mean flow, high-frequency eddies and surface boundary conditions could all be culprits of model biases in blocking frequency (e.g., Matsueda et al. 2009, Scaife et al. 2010, 2011). To this date, the most recent generation of global climate models, coupled model intercomparison project phase 5 (CMIP5), have not been validated in the context of NH blocking climatology.

The primary goal of this study is to provide a preliminary analysis of the performance of the CMIP5 models in reproducing NH blocking climatology. This is achieved by applying a relatively simple but comprehensive blocking index, used in chapter 3 of this work, to historical simulations. Only a subset of model data is currently available for widespread use. As such, this study utilizes historical simulations of 500-hPa geopotential height from only nine of the models (Table 4.1), which is to be extended to a larger number of model simulations in future work.

It should be noted that relatively few studies have been conducted for documenting the blocking response to anthropogenic forcings in the future climate. In fact, blocking was not commented upon in the IPCC AR4 report (Intergovernmental Panel on Climate Change, 2007). Of the few studies addressing this issue, Barnes and Hartmann [2010] and Barnes et al. [2011] report reductions in annual-mean NH blocking frequency in the CMIP3 integrations. This is in agreement with other individual models forced under global warming (e.g., Woollings 2010). There is, however, a disagreement concerning future changes in the duration of individual blocking events [Matsueda et al., 2009, Sillmann and Croci-Maspoli, 2009].

Extending these studies, we attempt to analyze predicted changes in blocking due to increased greenhouse gas (GHG) forcing in the CMIP5 models by directly comparing the blocking climatologies derived from historical runs to those obtained from RCP8.5 runs. Although only four models are available at this moment (Table 4.1), this comparison would be of significant value.

This chapter is organized as follows. The model data used in this study are briefly described in section 2. The 40-year (1966-2005) blocking climatologies derived from historical simulations from nine different models participating in CMIP5 are quantitatively compared with the blocking climatology obtained from NCEP-NCAR Reanalysis in section 3. It is followed by a comparison between 40-year blocking climatologies derived from forced RCP8.5 (2060-2099) and historical runs in section 4 to examine future changes in blocking as simulated by four models participating in CMIP5. Lastly, a summary and conclusions are given in section 5.

4.2 Data

The model data used in this study are historical and RCP8.5 integrations from a subset of the climate models participating in the coupled model inter-comparison project phase 5 (CMIP5) and are briefly listed in Table 4.1. Historical runs are 20th century integrations run with all observed forcings. The representative concentration pathway (RCP) experiments are labeled according to the approximate target radiative forcing at year 2100 (e.g., RCP8.5 identifies a concentration pathway that approximately results in a radiative forcing of 8.5 Wm^{-2} at year 2100, relative to pre-industrial conditions). Further details about the historical and RCP8.5 integration experiment set up can be found in Moss et al. [2010] and Taylor et al. [2012].

In this study, historical integrations from nine different models are used to assess the performance of the CMIP5 models in simulating the NH blocking climatology in the current climate. Forty-year integrations from 1966 to 2005 are quantitatively compared to NCEP-NCAR reanalysis for the same time period. The analysis is further extended to the NH future climate, where RCP8.5 integrations from four different models are used to examine possible changes in blocking frequency and duration in a warm climate. This is done by quantitatively comparing the blocking climatologies derived from forty-year RCP8.5 integrations from 2060-2099 to the historical integrations from the same models. In order to conduct these comparisons, all model and NNR data are linearly interpolated to the lowest model resolution in the subset of models used here, namely that of CanESM2 with a resolution of 2.8° latitude by 2.8° by longitude (Table 4.1).

4.3 Results

4.3.1 Blocking climatology in the current climate

The annual mean blocking frequencies for 9 CMIP5 models, derived from 40-year long data (1966-2006), are presented in Fig. 4.1 and compared with NNR. It can be seen that the models capture the overall geographical distribution of blocking frequency, namely the EA and PA action centers, reasonably well (Fig. 4.1b). However, noticeable differences are present. Most of all, the EA blocking frequency maxima is underestimated by about 40% in the multi-model mean. This feature is common to all the models analysed and is consistent with previous studies documenting blocking in earlier generations of GCMs (e.g., D'Andrea et al. 1998, Scaife et al. 2010). The blocking frequency bias over the Pacific, however, is not as clear across the models. Overestimation of blocking frequency is found in more than half the models resulting in slightly more frequent blocking over the Pacific in the multi-model mean in comparison to NNR.

The seasonal cycles of blocking frequency in NNR and the CMIP5 models are further examined in Fig. 4.2. It presents the monthly evolution of the NH blocking frequency as a function of longitude. Again, the longitudinal distribution of blocking frequency and their seasonality are reasonably well reproduced in the multi-model mean (Fig. 4.2b). It can be seen that the underestimation of EA blocking frequency is largely confined to the cold season whereas the overestimation of PA blocking frequency is observed throughout most of the year in the models. Peak PA blocking frequency is also delayed from January to February in the multi-model mean. Similarly, the models are able to reproduce the August PA peak in blocking frequency observed in the NNR, however, it is also delayed by one month into September.

It should be noted that the underestimation of blocking frequency over the Atlantic occurs irrespective of model resolution in IPSL-CM5A integrations (Fig. 4.1h,i). This is not consistent with Matsueda et al. [2009] who observed more accurate Euro-Atlantic blocking frequencies in higher resolution AGCM simulations. In fact, a moderate increase in horizontal resolution in IPSL-CM5A results in slightly poorer simulated blocking over the Euro-Atlantic. This result may support the recent finding of Scaife et al. [2011] who showed that Euro-Atlantic blocking frequency biases were largely dependent on surface ocean boundary conditions rather than the model horizontal resolution in the Hadley Centre Global Environmental Model version 3 (HadGEM3). Over the north-Pacific, IPSL-CM5A integrations are also inconsistent with the overestimation of Pacific blocking frequency observed in the high resolution model simulations of Matsueda et al. [2009]. Higher resolution models are not necessarily associated with overestimated Pacific blocking.

Figure 4.3 presents the annual number of NH blocking events as a function of duration for the CMIP5 models and NNR. The lifetime distribution of the multi-model mean blockings exhibits an exponential decrease with blocking persistence (Fig. 4.3a). This is in good agreement with the NNR. While there is a weak tendency in the underestimation of the number of short lived blockings (5-10 days), it is statistically insignificant in most of the models. The underestimation of the number of short lived blockings in some models may well result from the underestimation of the number of EA blocking events (Fig. 4.1). These results suggest the dominant error in model blocking frequency, as simulated by the CMIP5 models, is the misrepresentation of the numbe of EA and PA blocking events as opposed to blocking lifetime for the same number of blocking events.

4.3.2 Future changes in blocking climatology

The annual mean blocking frequency for four CMIP5 RCP8.5 integrations, derived from 40-year long data (2060-2099), are presented in Fig. 4.4

and compared with their historical simulations (1966-2005). It can be seen that the geographical distribution of blocking frequency in the forced simulations is quite similar to the current climate. Blocking frequencies over the PA sector and northern Canada, however, are slightly reduced in the future climate (compare Fig. 4.4a with 4.4b). Specifically, this feature is seen over the PA sector in all four models analysed. There is further evidence of a slight increase in Ural blocking frequencies shown in three of the four models. In contrast, there is no clear trend in future blocking activity over the EA sector.

The seasonal cycles of blocking frequency in the CMIP5 models are further compared with their historical simulations in Fig. 4.5. Again, it can be seen that the geographical distribution and seasonality in the forced simulations are quite similar to the current climate. In fact, the reduced blocking frequency over the PA sector is not as clear as that in Fig. 4.4. It is however noteworthy that decreases in blocking frequency occur throughout the year although this is statistically significant in only two of the four models. Slight increases in blocking frequency over the Ural mountain region can be seen in the multi-model mean (Fig. 4.5a). However, this is largely due to the biases in a single model (Fig. 4.5d).

Figure 4.6 presents the annual number of NH blocking events as a function of duration for both future and current climate simulations. The differences in the number of individual blocking events are largely statistically insignificant in all four models.

The above results do not provide any clear evidence of an overall decrease in NH blocking frequency or duration of individual blocking events under global warming, as shown in the previous studies (e.g., Barnes and Hartmann 2010, Matsueda et al. 2009), although it does suggest a slight decrease in future PA blocking frequency. However, this finding should be taken with a great caution, as more models are needed to achieve a robust conclusion.

4.4 Conclusion

In this study, preliminary analyses of Northern Hemisphere blocking climatology are undertaken using a subset of climate models participating in the coupled model inter-comparison project phase 5 (CMIP5). Both historical and RCP8.5 runs are examined to evaluate the performance of the CMIP5 models in comparison to NNR and to identify possible changes in blocking frequency and duration in a warm climate. This is achieved by applying the blocking index, used in chapter 3 of this work, to both model historical and RCP8.5 integrations.

Comparison to reanalysis data revealed that most CMIP5 models can reproduce the Northern Hemisphere blocking climatology reasonably well although maximum EA blocking frequency is generally underestimated. Significant overestimation of maximum PA blocking frequency is also evident in some models. The seasonal cycles of blocking frequency further show that the underestimation of EA blocking frequency is largely confined to the cold season whereas the overestimation of PA blocking frequency is observed throughout the year.

The RCP8.5 integrations show a weak hint of reduced blocking frequency over the PA sector as compared to historical integrations. No clear seasonality in PA blocking frequency change is observed. Additionally, no significant difference is found in terms of block duration within the RCP8.5 integrations. This result however should be taken with caution as only four models are analyzed. In future study, more models will be examined to get more robust results.

Table 4.1: Description of CMIP5 models used in chapter 4. Details of each model can be found at http://cmip-pcmdi.llnl.gov/cmip5/. Resolutions refer to atmospheric resolution and horizontal resolution is approximate for spectral models. The historical and RCP8.5 integration collumns refer to the runs used in this analysis.

Model	*Group, country*	*Horizontal res. (lat. x lon.)*	*Historical run*	*RCP8.5 run*
NorESM1-M	NCC, Norway	f19L26 (2.5°x1.875°)	yes	yes
HadGEM2-CC	MOHC, UK	N96L60 (1.875°x1.25°)	yes	yes
CanESM2	CCCma, Canada	T63L35 (2.8°x2.8°)	yes	yes
MRI-CGCM3	MRI, Japan	TL159L48 (1.125°x1.125°)	yes	yes
CNRM-CM5	CNRM, France	TL127L31 (1.4°x1.4°)	yes	no
IPSL-CM5A-LR	IPSL, France	(1.875°x3.75°)	yes	no
IPSL-CM5A-MR	IPSL, France	(1.25°x2.5°)	yes	no
MIROC5	CCSR, Japan	T85L40 (1.4°x1.4°)	yes	no
MIROC-ESM-CHEM	CCSR, Japan	T42L80 (2.8°x2.8°)	yes	no

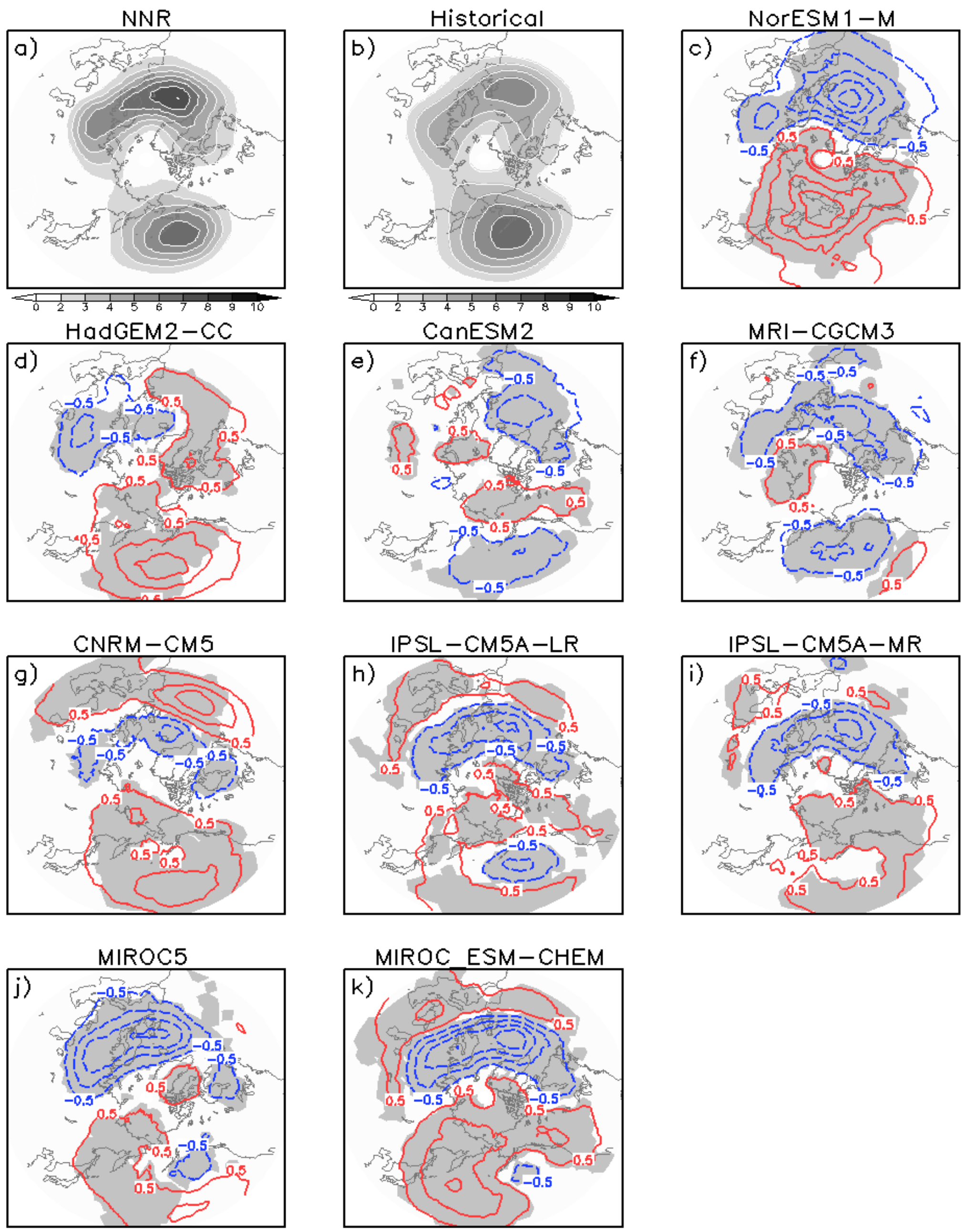

Figure 4.1: Climatology of NH annual-mean blocking frequency over the period of 1966-2006: (a) NNR, (b) CMIP5 historical simulation multi-model mean, and (c-k) individual model's biases as defined by model - NNR. Shading interval in (a,b) is in percent of days per year. Contour interval in (c-k) is 0.5 percent of days per year and zero lines are omitted. Shaded areas in (c-k) denote statistically significant differences at the 95 percent confidence level using a two-tailed student t-test.

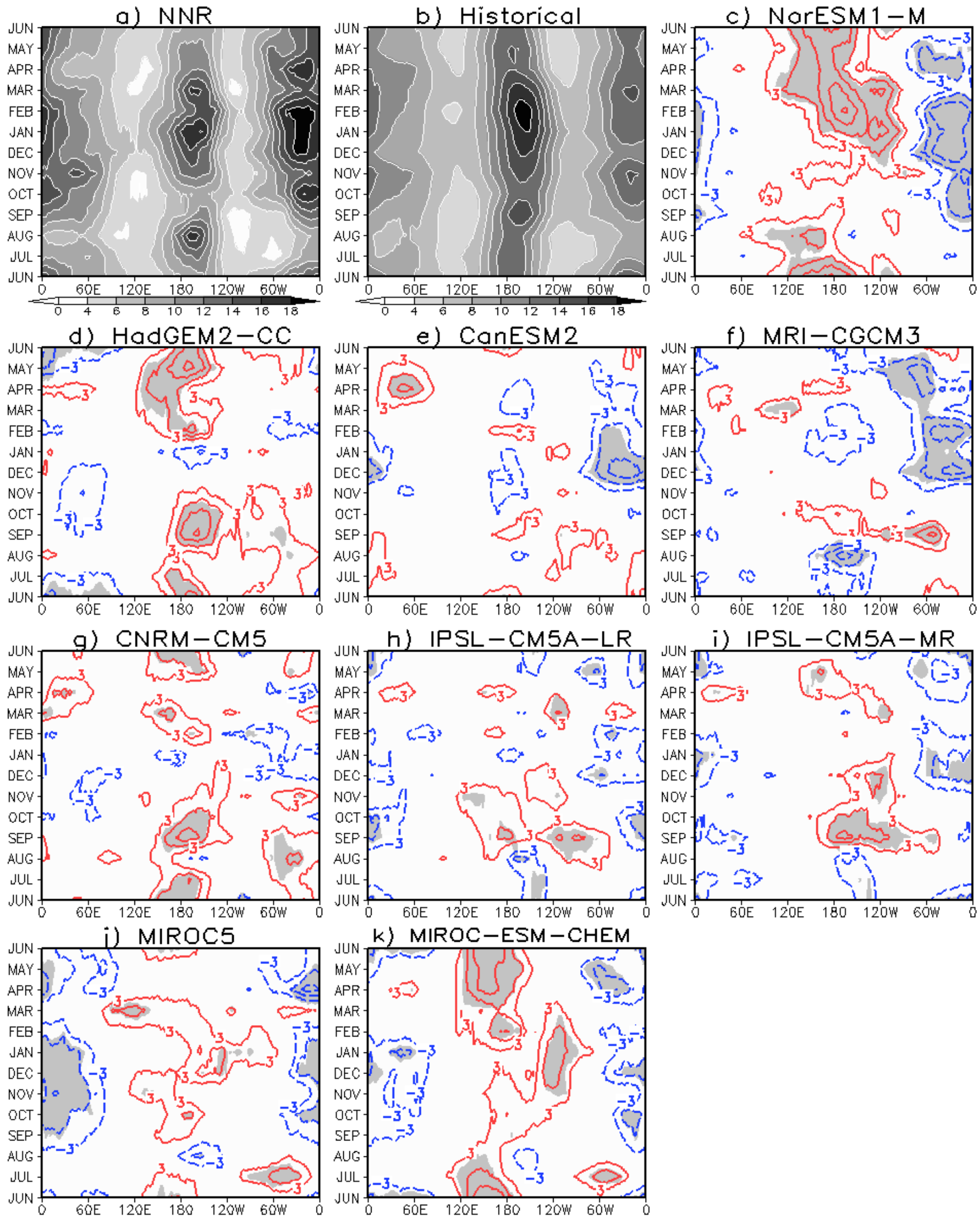

Figure 4.2: Seasonal cycle of the NH blocking frequency as a function of longitude: (a) NNR, (b) CMIP5 historical simulation multi-model mean, and (c-k) individual model's biases as defined by model - NNR. Shading interval in (a,b) is in percent of days per month. Contour interval in (c-k) is 3 percent of days per month and zero lines are omitted. Shaded areas in (c-k) denote statistically significant differences at the 95 percent confidence level using a two-tailed student t-test.

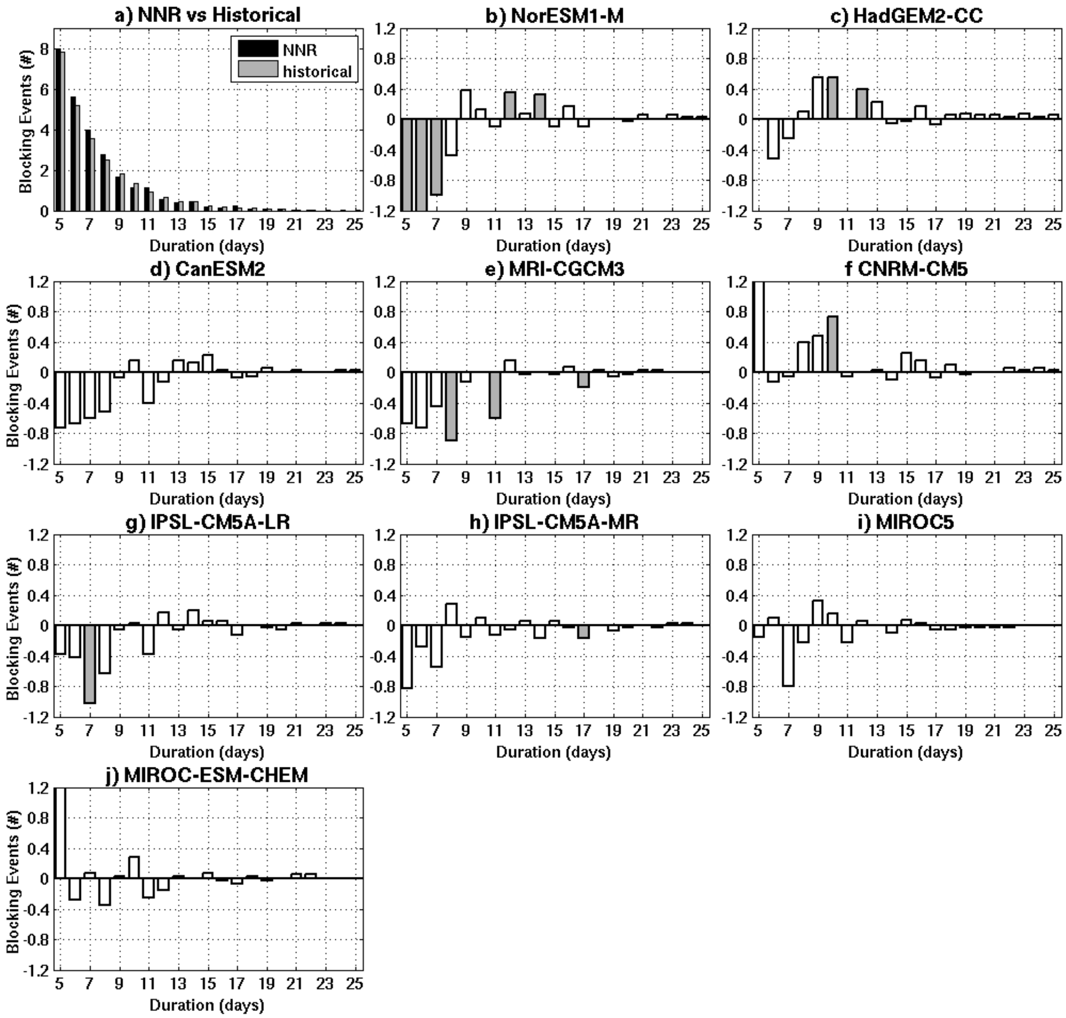

Figure 4.3: Annual mean number of NH blocking events as a function of duration: (a) NNR (black) and multi-model mean (grey bars), and (b-j) individual model biases as defined by model - NNR. Shaded bars in (b-j) denote statistically significant differences at the 95 percent confidence level using a two-tailed student t-test.

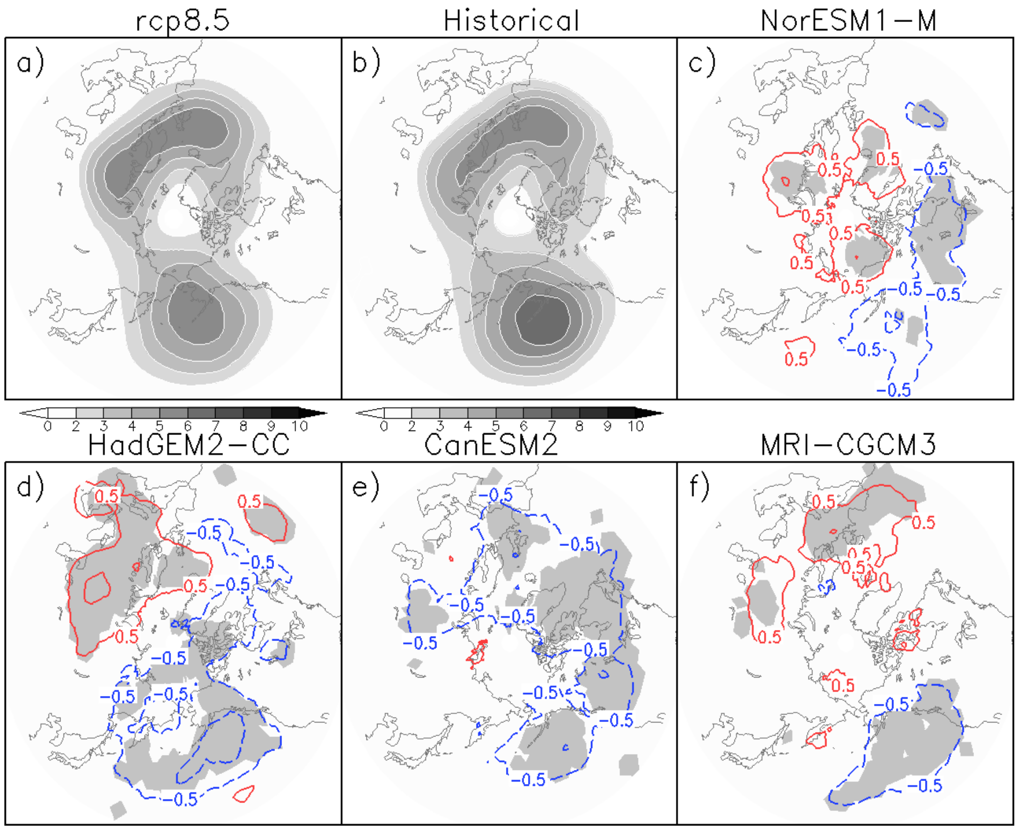

Figure 4.4: Climatology of NH annual-mean blocking frequency for the CMIP5 simulations: Multi-model mean for (a) RCP8.5 (1966-2005), (b) historical simulations (1960-2099) and (c-f) individual model biases as defined by RCP8.5 - historical runs. Shading interval in (a,b) is in percent of days per year. Contour interval in (c-f) is 0.5 percent of days per year and zero lines are omitted. Shaded areas in (c-f) denote statistically significant differences at the 95 percent confidence level using a two-tailed student t-test.

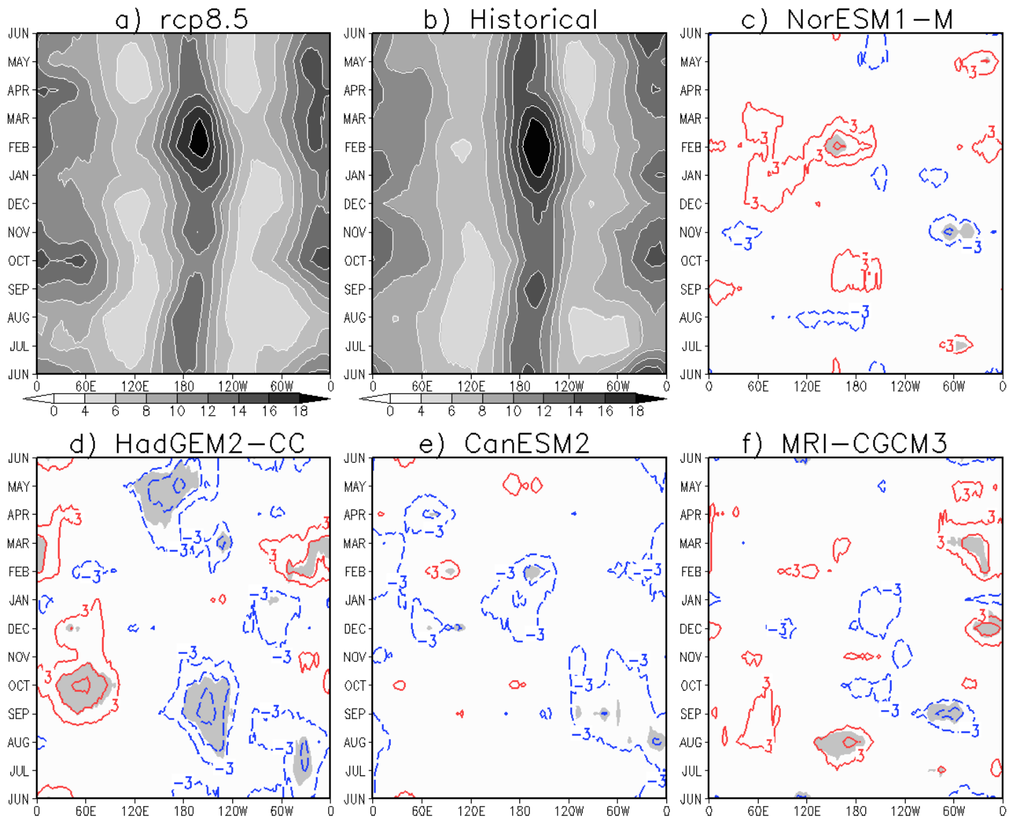

Figure 4.5: Seasonal cycle of the NH blocking frequency as a function of longitude for the CMIP5 simulations: Multi-model mean for (a) RCP8.5, (b) historical simulations and (c-f) individual model biases as defined by RCP8.5 - historical runs. Shading interval in (a,b) is in percent of days per month. Contour interval in (c-f) is 3 percent of days per month and zero lines are omitted. Shaded areas in (c-f) denote statistically significant differences at the 95 percent confidence level using a two-tailed student *t*-test.

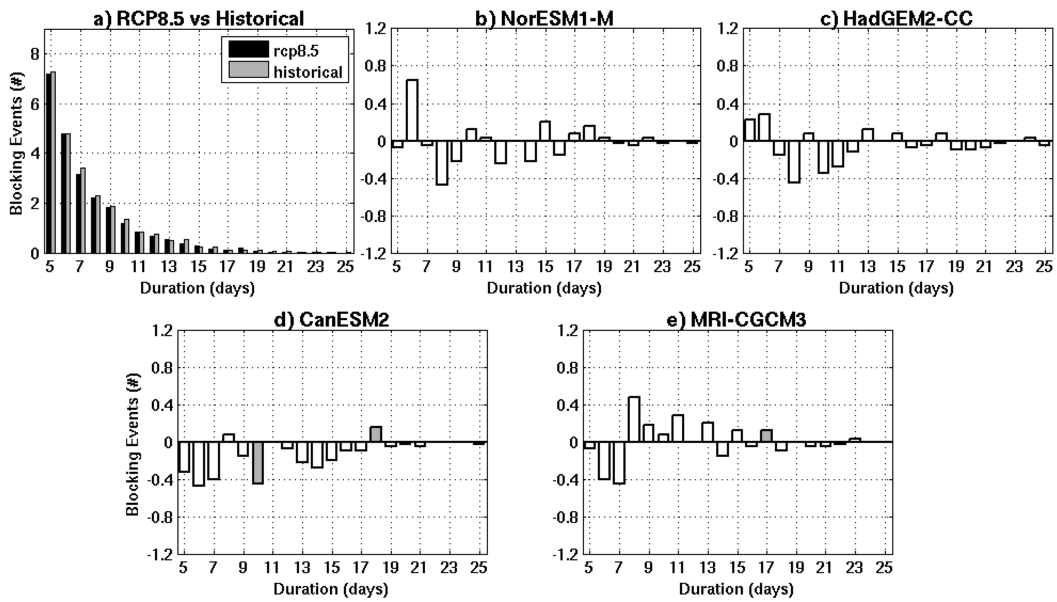

Figure 4.6: Annual mean number of NH blocking events as a function of duration for the CMIP5 simulations: Multi-model mean of the models in (b-e) for (a) RCP8.5 (black) and historical (grey bars), and (b-e) individual model differences defined by RCP8.5 - historical. Shaded bars in (b-e) denote statistically significant differences at the 95 percent confidence level using a two-tailed student t-test.

Chapter 5

Conclusion

In the first part of this work, the performance of the Global Environmental Multiscale (GEM) model is evaluated in this study in the context of the Northern Hemisphere (NH) blocking climatology. Geographical distribution, seasonal cycle and statistics of individual blocking events are quantitatively compared with those derived from the NCEP-NCAR Reanalysis (NNR). This comparison is conducted by applying a newly developed blocking index to the GEM and NNR data in a same resolution.

The blocking index developed in this study is a kind of hybrid index which combines the two widely-used blocking indices, namely the Dole-Gordon and Tibaldi-Molteni indices, in a simple way. Specifically blocking highs are identified by assuring the latitudinal gradient reversal in 500-hPa geopotential height field, as in the Tibaldi-Molteni type index, on the equatorward side of blocking anomalies which are defined by the Dole-Gordon type index. This approach effectively removes quasi-stationary ridges that are often mis-detected as blockings in the Dole-Gordon type index. It also allows us to detect omega-shape blockings which are often ignored in the Tibaldi-Molteni type index.

It is found that the GEM model is able to reproduce individual blocking events reasonably well. The total number of NH blocking events and their duration and intensity are quantitatively well simulated in comparison to the NNR. However, significant biases are found in blocking frequency over the two basins with seasons. The biases can be summarized in three key aspects: (1) The peak season of blocking activity is delayed from winter to early spring in both basins. (2) The Euro-Atlantic (EA) blocking frequency is generally underestimated in the cold season. (3) The north Pacific (PA) blocking frequency is overestimated in most seasons. The last point, the overestimate of the PA blockings, is the most peculiar finding in this study as numerical models typically underestimate blocking activity over both the Euro-Atlantic and north Pacific basins [Barriopedro et al., 2010a, D'Andrea et al., 1998, Doblas-Reyes et al., 2002, Scaife et al., 2010]. Although Matsueda et al. [2009] showed an example of overestimated PA blocking frequency in their model, it was found only in a very high-resolution model integration, much higher than the one used in the GEM model.

The model blocking biases are found to be largely associated with the biases in the time mean flow. More specifically stationary wave activity in the model exhibits a seasonal delay and equatorward shift in zonal wavenumber one component. This is consistent with the seasonal delay in maximum blocking frequency in both basins. In high latitudes, zonal wavenumber two component shows an eastward shift, yielding a deeper than normal trough over the north Pacific and shallower than normal trough over the north Atlantic. This likely results in a stronger interaction between quasi-stationary waves and transient waves over the north Pacific but a weaker interaction over the north Atlantic, possibly explaining anomalous blocking activity over the two basins with opposite sign during most seasons. Although this does not provide a causal relationship as the mean-flow biases may simply result from the blocking biases themselves, a similar consistency is not found in high-frequency eddies which are underestimated over both basins in most seasons. This indicates that the possible non-linear energy transfer from high-frequency transient eddies to quasi-stationary blocking anomalies may not be a direct cause of the overestimate of PA blocking in ONDJ and the seasonal delay in PA and EA blocking in late winter, although it may play a role in cold season EA blocking which is underestimated by the model.

The importance of the time-mean flow in blocking biases is further supported by the energetics. It is particularly found that the model biases in PA blocking frequency are consistent with barotropic energy conversion from the mean flow to low-frequency eddies. The model shows an southeastward extension of the Pacific jet in most seasons. Westerly biases are also evident over Europe in the cold season. These biases result in stronger (weaker) stretching deformation over the north Pacific (eastern Atlantic-Europe), causing stronger (weaker) barotropic energy transfer from the time-mean flow to the low-frequency eddies there. However a corresponding energy transfer for the EA sector in March and April is not clear.

The causes of time-mean flow and transient eddy biases, which are inherently linked to blocking biases as summarized above, are not addressed in this study. They could result from insufficient model resolution, unrealistic physics, prescribed (not interactive) surface boundary conditions, etc. To address these issues, systematic model sensitivity tests would be needed. This is however beyond the scope of the present study.

It should be stated that overall results reported here could be sensitive to the choice of blocking index. In fact, north Pacific blocking biases become much smaller when a classical Tibaldi-Molteni index is applied. This likely results from the ignorance of omega shaped blocking in the Tibaldi-Molteni index. Likewise, if a blocking index is applied to a dynamic variable in the upper troposphere (e.g., potential vorticity on the 2 PVU surface), instead of a thermodynamic variable in the mid-troposphere as done in this study, quantitatively different results could emerge. However, given the similarity between the blocking climatology found in this study and low-frequency variability at 500 hPa (Figs. 3.7c and 3.15c), we believe that overall results would not change in quality.

In the second part of this work, preliminary analyses of Northern Hemisphere blocking climatology are undertaken using a subset of climate models participating in the coupled model inter-comparison project phase 5 (CMIP5). Both historical and RCP8.5 runs are examined to evaluate the performance of the CMIP5 models in comparison to NNR and to identify possible changes in blocking frequency and duration in a warm climate. This is achieved by applying the blocking index, used in chapter 3 of this work, to both model historical and RCP8.5 integrations.

Comparison to reanalysis data revealed that most CMIP5 models can reproduce the Northern Hemisphere blocking climatology reasonably well although maximum EA blocking frequency is generally underestimated. Significant overestimation of maximum PA blocking frequency is also evident in some models. The seasonal cycles of blocking frequency further show that the underestimation of EA blocking frequency is largely confined to the cold season whereas the overestimation of PA blocking frequency is observed throughout the year.

The RCP8.5 integrations show a weak hint of reduced blocking frequency over the PA sector as compared to historical integrations. No clear seasonality PA blocking frequency change is observed. Additionally, no significant difference is found in terms of block duration within the RCP8.5 integrations. This result however should be taken with caution as only four models are analyzed. In a future study, more models will be examined to get more robust results.

Appendix

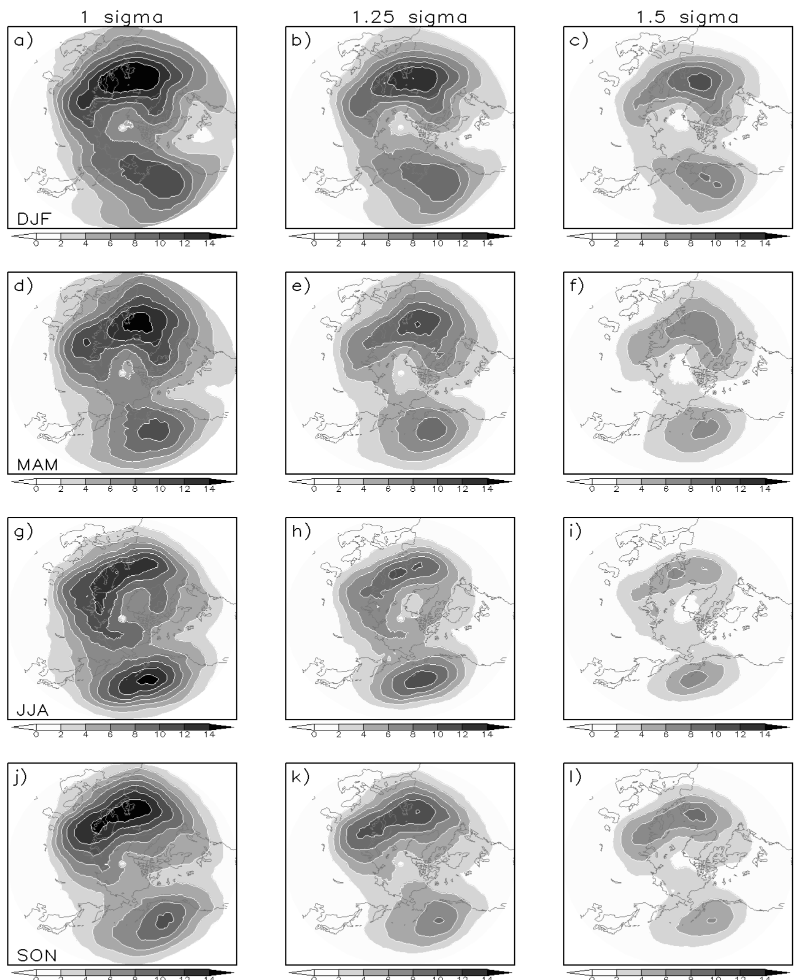

Figure A.1: Climatology of seasonal-mean NH blocking frequency for 50-year NNR using amplitude threshold (A) of (a,d,g,j) 1 standard deviation, (b,e,h,k) 1.25 standard deviation and (c,f,i,l) 1.5 standard deviation with all other thresholds as in this study: (a-c) DJF, (d-f) MAM, (g-i) JJA and (j-l) SON. Shading interval is in percent of days per season.

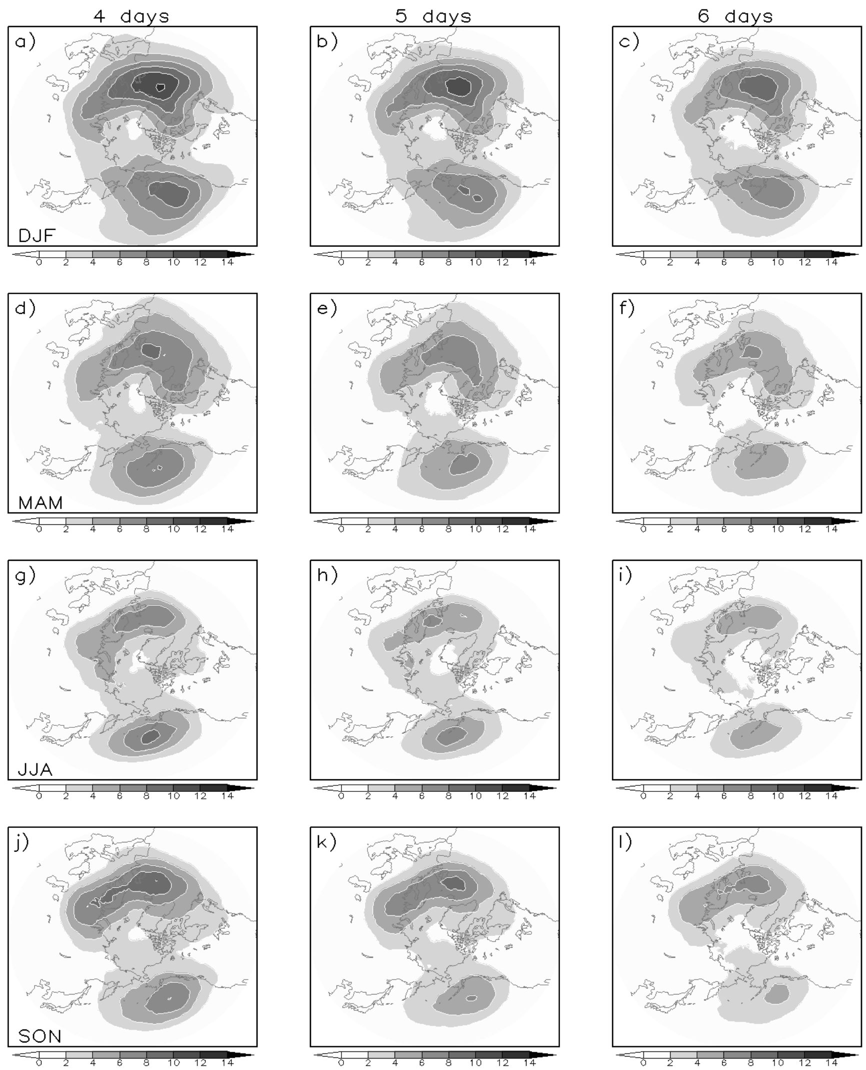

Figure A.2: Same as Fig. A.1 except with varied duration criteria (D) of (a,d,g,j) 4 days, (b,e,h,k) 5 days and (c,f,i,l) 6 days.

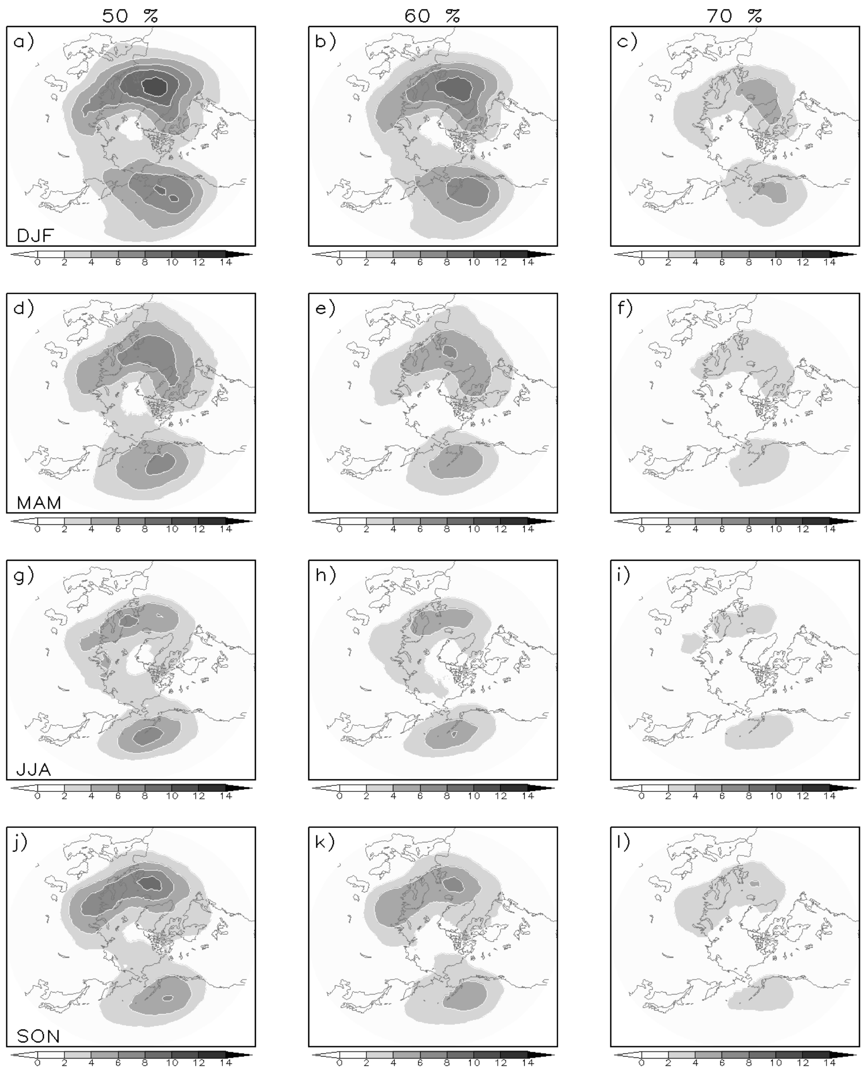

Figure A.3: Same as Fig. A.1 except with varied overlap threshold (O) of (a,d,g,j) 50%, (b,e,h,k) 60% and (c,f,i,l) 70%.

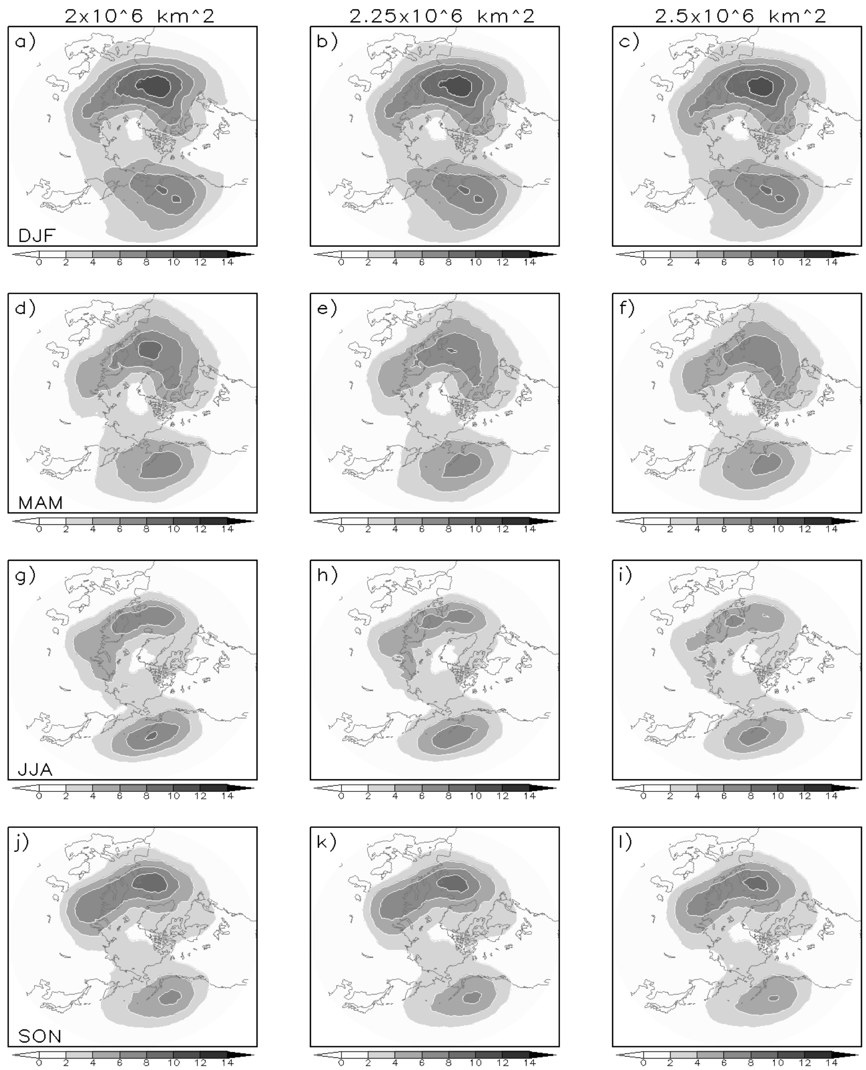

Figure A.4: Same as Fig. A.1 except with varied spatial threshold (S) of (a,d,g,j) $2x10^6$ km^2, (b,e,h,k) $2.25x10^6$ km^2 and (c,f,i,l) $2.5x10^6$ km^2.

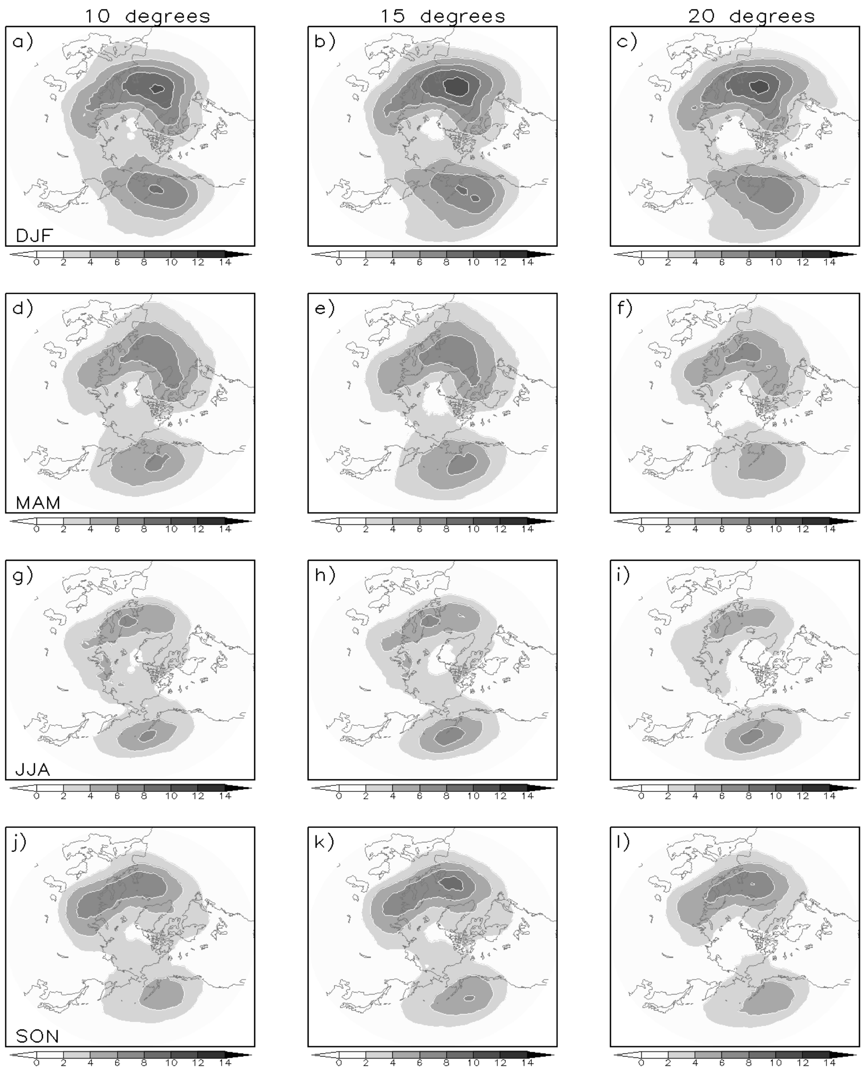

Figure A.5: Same as Fig. A.1 except with varied meridional scale $\Delta\phi$ of (a,d,g,j) 10°, (b,e,h,k) 15° and (c,f,i,l) 20° latitude.

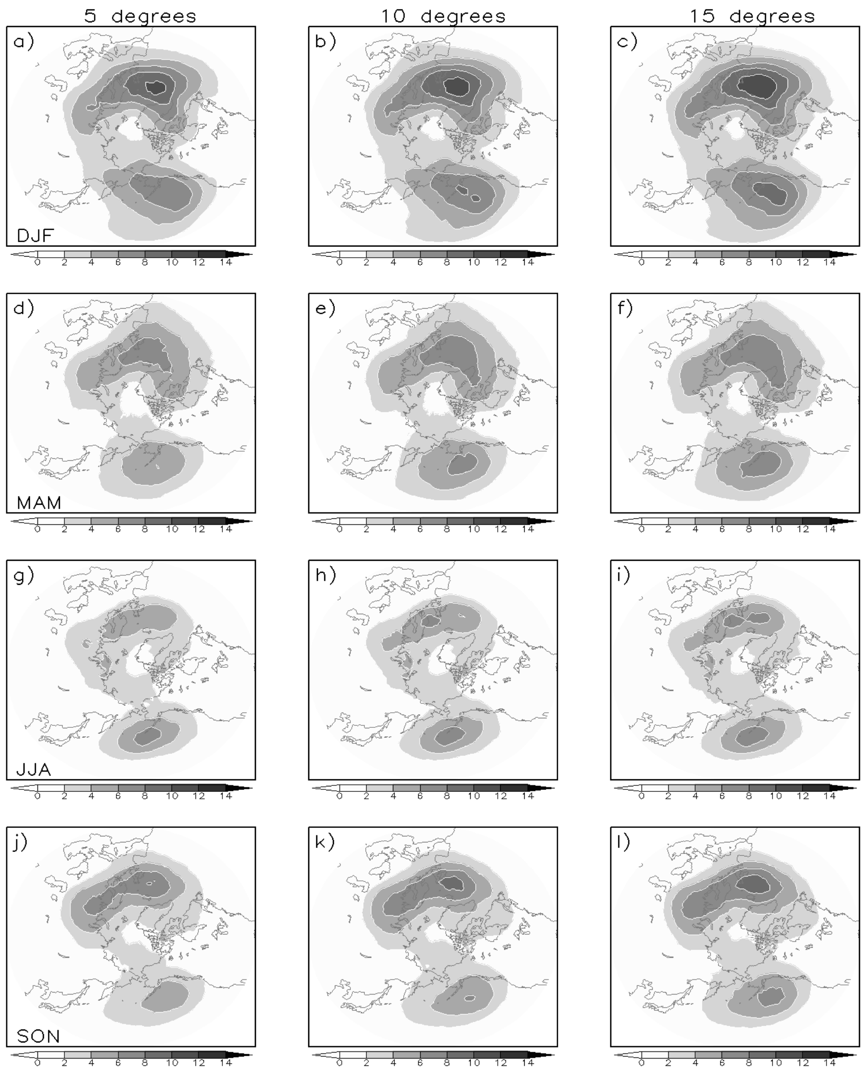

Figure A.6: Same as Fig. A.1 except with varied zonal scale $\Delta\lambda$ of (a,d,g,j) 5°, (b,e,h,k) 10° and (c,f,i,l) 15° longitude.

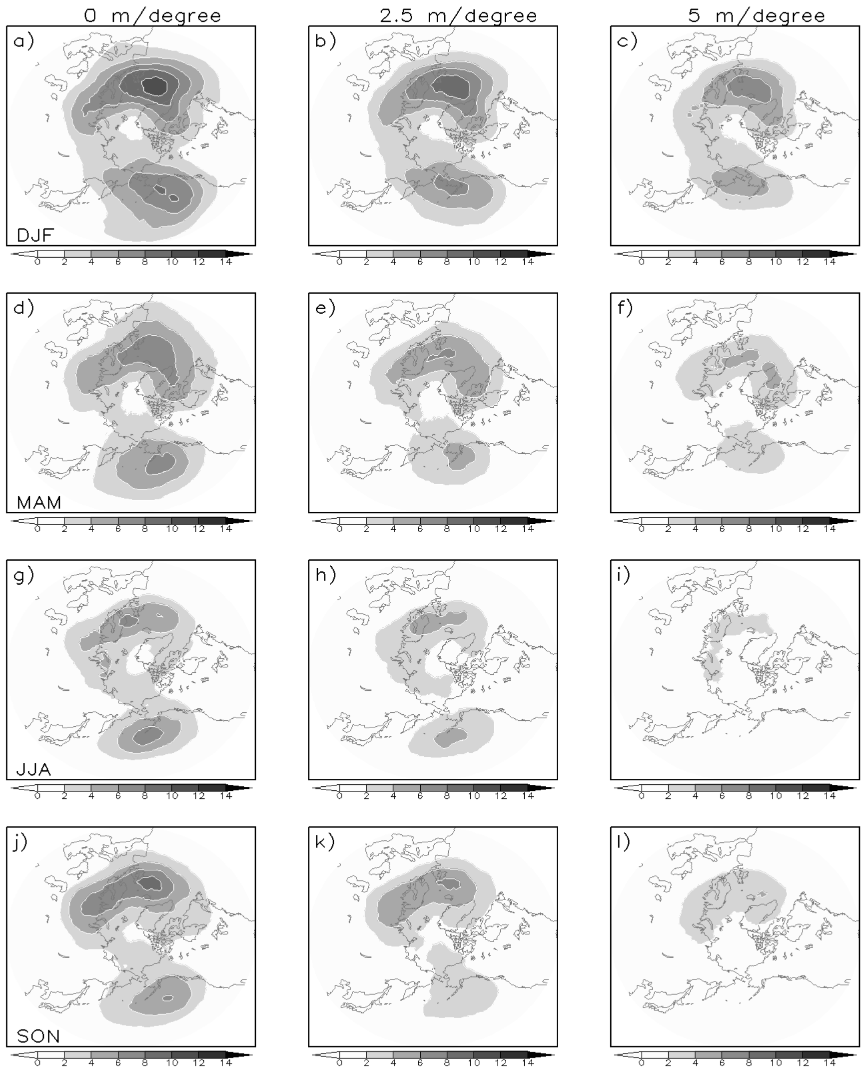

Figure A.7: Same as Fig. A.1 except with varied meridional geopotential height gradient threshold $Gr(i^*)$ of (a,d,g,j) 0 $m\ deg^{-1}$, (b,e,h,k) 2.5 $m\ deg^{-1}$ and (c,f,i,l) 5 $m\ deg^{-1}$ longitude.

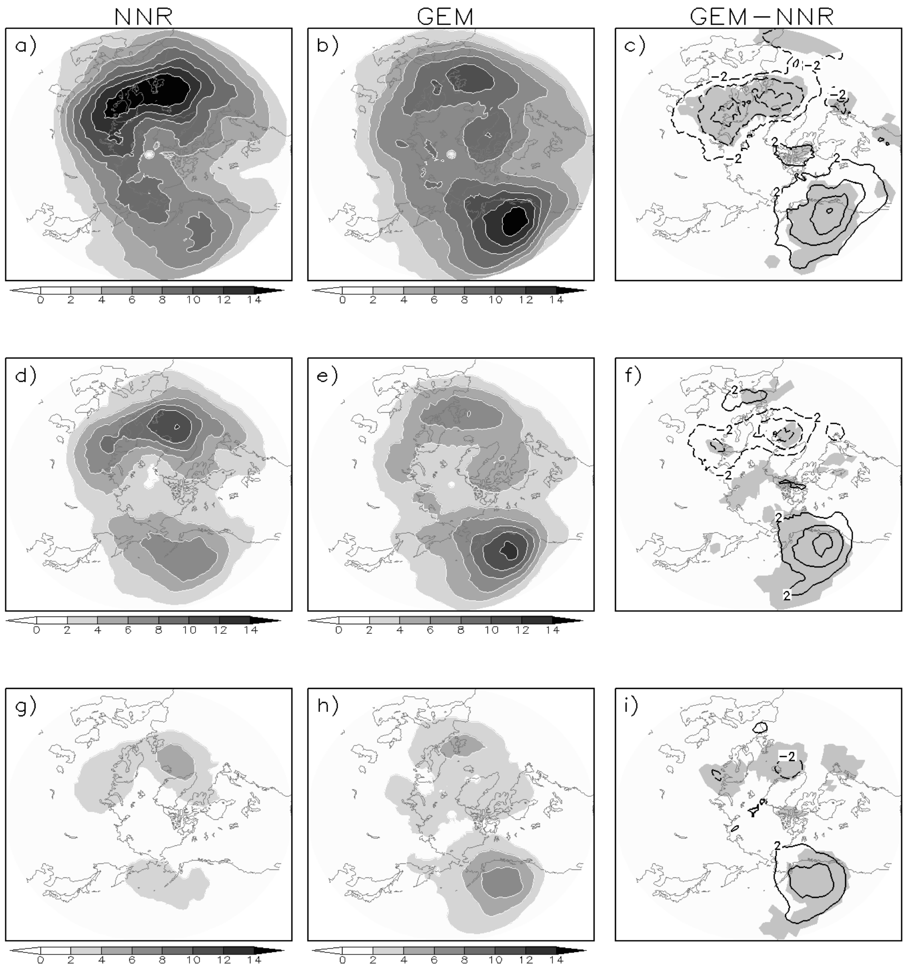

Figure A.8: Climatology of NH blocking frequency for (a-c) amplitude threshold of 1 standard deviation, (d-f) duration criteria of 4 days and (g-i) overlap threshold of 70% with all other criteria as before: (a,d,g) NNR, (b,e,h) GEM model and (c,f,i) their difference during ONDJ. Shading is in units of percent of days per season. Contour interval in (c,f,i) is 2 percent and the zero lines are omitted. Values which are statistically significant at the 95 percent confidence level using a two-tailed t-test are shaded.

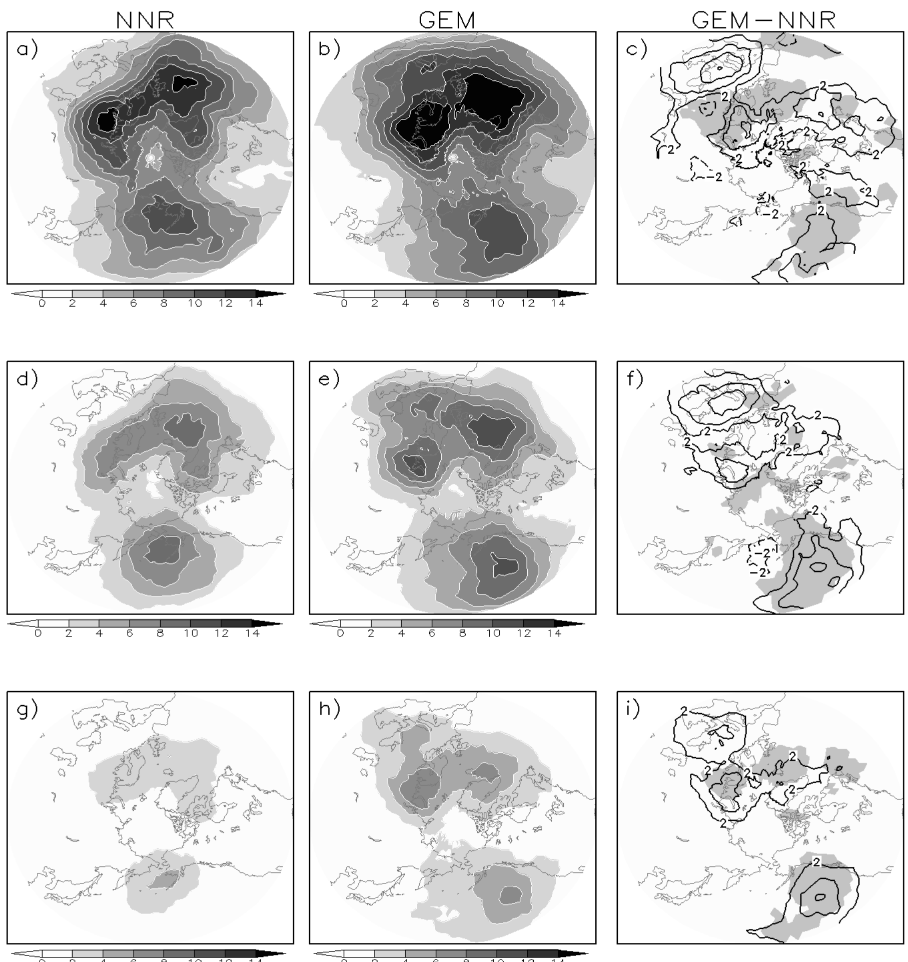

Figure A.9: Same as Fig. A.8 except for MA.

Bibliography

Altenhoff, A. M., O. Martius, M. Croci-Maspoli, C. Schwierz, and H. C. Davies, 2008: Linkage of atmospheric blocks and synoptic-scale Rossby waves: a climatological analysis. *Tellus*, **60**, 1053–1063.

Austin, J. F., 1980: The blocking of middle latitude westerly winds by planetary-waves. *Quart. J. Roy. Meteor. Soc.*, **106**, 327–350.

Barnes, E. A. and D. L. Hartmann, 2010: Influence of eddy-driven jet latitude on North Atlantic jet persistence and blocking frequency in CMIP3 integrations. *Geophys. Res. Lett.*, **37**, doi:10.1029/2010GL045700.

Barnes, E. A., J. Slingo, and T. Woollings, 2011: A methodology for the comparison of blocking climatologies across indices, models and climate scenarios. *Clim. Dynam.*, **23**, 1–15.

Barriopedro, D., R. Garcia-Herrera, J. F. Gonzalez-Rouco, and R. M. Trigo, 2010a: Application of blocking diagnosis methods to General Circulation Models. part II: model simulations. *Clim. Dynam.*, **35**, 1393–1409.

Barriopedro, D., R. Garcia-Herrera, and R. M. Trigo, 2010b: Application of blocking diagnosis methods to General Circulation Models. part I: a novel detection scheme. *Clim. Dynam.*, **35**, 1373–1391.

Berggren, R., B. Bolin, and C.-G. Rossby, 1949: An aerological study of zonal motion, its perturbations and break-down. *Tellus*, **1**, 14–37.

Berrisford, P., B. J. Hoskins, and E. Tyrlis, 2007: Blocking and Rossby wave breaking on the dynamical tropopause in the Southern Hemisphere. *J. Atmos. Sci.*, **64**, 2881–2898.

Black, E., M. Blackburn, G. Harrison, B. Hoskins, and J. Methven, 2004: Factors contributing to the summer 2003 European heatwave. *Weather*, **59**, 217–223.

Cash, B. and S. Lee, 2000: Dynamical processes of block evolution. *J. Atmos. Sci.*, **57**, 3202–3218.

Charney, J. and J. Devore, 1979: Multiple flow equilibria in the atmosphere and blocking. *J. Atmos. Sci.*, **36**, 1205–1216.

Colucci, S., 1985: Explosive cyclogenesis and large-scale circulation changes - implications for atmospheric blocking. *J. Atmos. Sci.*, **42**, 2701–2717.

Colucci, S. J., A. Z. Loesch, and L. F. Bosart, 1981: Spectral evolution of a blocking episode and comparison with wave interaction theory. *J. Atmos. Sci.*, **38**, 2092–2111.

Côte, J., J. Desmarais, S. Gravel, A. Methot, A. Patoine, M. Roch, and A. Staniforth, 1998a: The operational CMC-MRB Global Environmental Multiscale (GEM) model. part II: Results. *Mon. Wea. Rev.*, **126**, 1397–1418.

Côte, J., S. Gravel, A. Methot, A. Patoine, M. Roch, and A. Staniforth, 1998b: The operational CMC-MRB Global Environmental Multiscale

(GEM) model. part I: Design considerations and formulation. *Mon. Wea. Rev.*, **126**, 1373–1395.

Croci-Maspoli, M., C. Schwierz, and H. C. Davies, 2007a: Atmospheric blocking: space-time links to the NAO and PNA. *Clim. Dynam.*, **29**, 713–725.

Croci-Maspoli, M., C. Schwierz, and H. C. Davies, 2007b: A multifaceted climatology of atmospheric blocking and its recent linear trend. *J. Climate*, **20**, 633–649.

D'Andrea, F., et al., 1998: Northern Hemisphere atmospheric blocking as simulated by 15 atmospheric general circulation models in the period 1979-1988. *Clim. Dynam.*, **14**, 385–407.

Diao, Y., J. Li, and D. Luo, 2006: A new blocking index and its application: Blocking action in the Northern Hemisphere. *J. Climate*, **19**, 4819–4839.

Doblas-Reyes, F., M. Casado, and M. Pastor, 2002: Sensitivity of the Northern Hemisphere blocking frequency to the detection index. *J. Geophys. Res.*, **107**, doi:10.1029/2000JD000290.

Dole, R. and N. Gordon, 1983: Persistent anomalies of the extratropical Northern Hemisphere wintertime circulation - geographical-distribution and regional persistence characteristics. *Mon. Wea. Rev.*, **111**, 1567–1586.

Dole, R., et al., 2011: Was there a basis for anticipating the 2010 Russian heat wave? *Geophys. Res. Lett.*, **38**, doi:10.1029/2010GL046582.

Egger, J., 1978: Dynamics of blocking highs. *J. Atmos. Sci.*, **35**, 1788–1801.

Elliott, R. and T. Smith, 1949: A study of the effects of large blocking highs on the general circulation in the northern-hemisphere westerlies. *J. Meteor.*, **6**, 67–85.

Green, J., 1977: The weather during July 1976: some dynamical considerations of the drought. *Weather*, **32**, 120–126.

Hansen, A. and A. Sutera, 1984: A comparison of the spectral energy and enstrophy budgets of blocking versus nonblocking periods. *Tellus*, **36**, 52–63.

Hansen, A. and A. Sutera, 1993: A comparison between planetary-wave flow regimes and blocking. *Tellus*, **45A**, 281–288.

Hoskins, B., I. James, and G. White, 1983: The shape, propagation and mean-flow interaction of large-scale weather systems. *J. Atmos. Sci.*, **40**, 1595–1612.

Hu, Y., D. Yang, and J. Yang, 2008: Blocking systems over an aqua planet. *Geophys. Res. Lett.*, **35**, doi:10.1029/2008GL035351.

Illari, L., 1984: A diagnostic study of the potential vorticity in a warm blocking anticyclone. *J. Atmos. Sci.*, **41**, 3518–3526.

Jia, X., J. Derome, and H. Lin, 2007: Comparison of the life cycles of the NAO using different definitions. *J. Climate*, **20**, 5992–6011.

Kaas, E. and G. Branstator, 1993: The relationship between a zonal index and blocking activity. *J. Atmos. Sci.*, **50**, 3061–3077.

Kalnay, E., et al., 1996: The NCEP/NCAR 40-year reanalysis project. *Bull. Amer. Meteor. Soc.*, **77**, 437–471.

Lejenas, H. and H. Okland, 1983: Characteristics of northern hemisphere blocking as determined from a long-time series of observational data. *Tellus*, **35**, 350–362.

Liu, Q., 1994: On the definition and persistence of blocking. *Tellus*, **46**, 286–298.

Martius, O., L. M. Polvani, and H. C. Davies, 2009: Blocking precursors to stratospheric sudden warming events. *Geophys. Res. Lett.*, **36**, doi: 10.1029/2009GL038776.

Matsueda, M., 2011: Predictability of Euro-Russian blocking in summer of 2010. *Geophys. Res. Lett.*, **38**, doi:10.1029/2010GL046557.

Matsueda, M., R. Mizuta, and S. Kusunoki, 2009: Future change in wintertime atmospheric blocking simulated using a 20-km-mesh atmospheric global circulation model. *J. Geophys. Res.*, **114**, doi:10.1029/2009JD011919.

Metz, W., 1986: Transient cyclone-scale vorticity forcing of blocking highs. *J. Atmos. Sci.*, **43**, 1467–1483.

Moss, R. H., et al., 2010: The next generation of scenarios for climate change research and assessment. *Nature*, **463**, 747–756.

Mullen, S., 1987: Transient eddy forcing of blocking flows. *J. Atmos. Sci.*, **44**, 3–22.

Nakamura, H., M. Nakamura, and J. Anderson, 1997: The role of high- and low-frequency dynamics in blocking formation. *Mon. Wea. Rev.*, **125**, 2074–2093.

Pelly, J. and B. Hoskins, 2003: A new perspective on blocking. *J. Atmos. Sci.*, **60**.

Renwick, J. and J. Wallace, 1996: Relationships between North Pacific wintertime blocking, El Nino, and the PNA pattern. *Mon. Wea. Rev.*, **124**, 2071–2076.

Rex, D. F., 1950a: Blocking action in the middle troposphere and its effect upon regional climate. part 1: An aerological study of blocking action. *Tellus*, **2**, 196–211.

Rex, D. F., 1950b: Blocking action in the middle troposphere and its effect upon regional climate. part 2: The climatology of blocking action. *Tellus*, **2**, 275–301.

Ringer, M., et al., 2006: The physical properties of the atmosphere in the new hadley centre global environmental model (HadGEM1). part II: Aspects of variability and regional climate. *J. Climate*, **19**, 1302–1326.

Sausen, R., W. Konig, and F. Sielman, 1995: Analysis of blocking events from observations and ECHAM model simulations. *Tellus*, **47**, 421–438.

Scaife, A. A., T. Woollings, J. Knight, G. Martin, and T. Hinton, 2010: Atmospheric blocking and mean biases in climate models. *J. Climate*, **23**, 6143–6152.

Scaife, A. A., et al., 2011: Improved Atlantic winter blocking in a climate model. *Geophys. Res. Lett.*, **38**, doi:10.1029/2011GL049573.

Scherrer, S., M. Croci-Maspoli, C. Schwierz, and C. Appenzeller, 2006: Two-dimensional indices of atmospheric blocking and their statistical relationship with winter climate patterns in the Euro-Atlantic region. *Int. J. Climatol.*, **26**, 233–249.

Schwierz, C., M. Croci-Maspoli, and H. Davies, 2004: Perspicacious indicators of atmospheric blocking. *Geophys. Res. Lett.*, **31**, doi: 10.1029/2003GL019341.

Sheng, J. and J. Derome, 1991a: An observational study of the energy-transfer between the seasonal mean flow and transient eddies. *Tellus*, **43**, 128–144.

Sheng, J. and J. Derome, 1991b: On the interactions among flow components in different frequency bands in the Canadian-Climate-Center General-Circulation Model. *Atmos.-Ocean*, **29**, 62–84.

Sheng, J. and Y. Hayashi, 1990a: Estimation of atmospheric energetics in the frequency-domain during the FGGE year. *J. Atmos. Sci.*, **47**, 1255–1268.

Sheng, J. and Y. Hayashi, 1990b: Observed and simulated energy cycles in the frequency-domain. *J. Atmos. Sci.*, **47**, 1243–1254.

Shutts, G., 1983: The propagation of eddies in diffluent jetstreams - eddy vorticity forcing of blocking flow-fields. *Quart. J. Roy. Meteor. Soc.*, **109**, 737–761.

Sillmann, J. and M. Croci-Maspoli, 2009: Present and future atmospheric blocking and its impact on European mean and extreme climate. *Geophys. Res. Lett.*, **36**, doi:10.1029/2009GL038259.

Simmons, A., J. Wallace, and G. Branstator, 1983: Barotropic wave-propagation and instability, and atmospheric teleconnection patterns. *J. Atmos. Sci.*, **40**, 1363–1392.

Solomon, S., D. Qin, M. Manning, Z. Chen, M. Marquis, K. B. Averyt, M. Tignor, and H. L. Miller, 2007: Climate change 2007 - the physical science basis: Working group I contribution to the fourth assessment report of the IPCC. *Cambridge University Press*.

Stein, O., 2000: The variability of Atlantic-European blocking as derived from long SLP time series. *Tellus*, **52**, 225–236.

Taylor, K. E., R. J. Stouffer, and G. a. Meehl, 2012: A summary of the CMIP5 experiment design. URL `Available online at http://cmip-pcmdi.llnl.gov/cmip5/experiment-design.html`.

Tibaldi, S., F. DAndrea, E. Tosi, and E. Roeckner, 1997: Climatology of Northern Hemisphere blocking in the ECHAM model. *Clim. Dynam.*, **13**, 649–666.

Tibaldi, S. and F. Molteni, 1990: On the operational predictability of blocking. *Tellus*, **42**, 343–365.

Trigo, R., I. Trigo, C. DaCamara, and T. Osborn, 2004: Climate impact of the European winter blocking episodes from the NCEP/NCAR Reanalyses. *Clim. Dynam.*, **23**, 17–28.

Tung, K. and R. Lindzen, 1979: Theory of stationary long waves .1. simple theory of blocking. *Mon. Wea. Rev.*, **107**, 714–734.

Tyrlis, E. and B. J. Hoskins, 2008: Aspects of a Northern Hemisphere atmospheric blocking climatology. *J. Atmos. Sci.*, **65**, 1638–1652.

Wallace, J. and H. Hsu, 1985: Another look at the index cycle. *Tellus*, **37**, 478–486.

Wallace, J. and N. Lau, 1985: On the role of barotropic energy conversions in the general-circulation. *Adv. Geophys.*, **28 (Part a)**, 33–74.

Webster, P. J., V. E. Toma, and H. M. Kim, 2011: Were the 2010 Pakistan floods predictable? *Geophys. Res. Lett.*, **38**, doi:10.1029/2010GL046346.

Woollings, T., 2010: Dynamical influences on European climate: an uncertain future. *Philos. Trans. Roy. Soc. London A*, **368**, 3733–3756.

Woollings, T., A. Charlton-Perez, S. Ineson, A. G. Marshall, and G. Masato, 2010: Associations between stratospheric variability and tropospheric blocking. *J. Geophys. Res.*, **115**, doi:10.1029/2009JD012742.

Woollings, T., B. Hoskins, M. Blackburn, and P. Berrisford, 2008: A new Rossby wave-breaking interpretation of the North Atlantic Oscillation. *J. Atmos. Sci.*, **65**, 609–626.